공학박사학위논문

# Characterization of negative electrodes prepared from fabric-shaped current collectors

# 직물 형태의 집전체를 이용하여 제작한 음극의 특성 평가

2017년 2월


**서울대학교 대학원**

화학생물공학부

**황 홍 서**

# Abstract

Negative electrode of lithium-ion batteries are composed of active material, binder, conducting agent and current collector. In this work, the materially and structurally distinguishable current collectors are utilized to make advanced negative electrodes. First, carbon fabric is used as a current collector to make the high specific capacity negative electrode. Secondly, stainless steel (SUS) fabric is utilized as a current collector to fabricate the flexible and high rate capable negative electrode.

$Cu_6Sn_5$-deposited carbon fiber paper (carbon fabric) is prepared successfully to develop high capacity negative electrode. Graphite is well-known to be highly electric conductive material, and it has a potential to be used as a current collector. When using graphite as a current collector, it is not only acting as a conventional current collector but reacting with lithium ion. In this study, carbon fabric is chosen as a current collector to increase overall electrode capacity. In the case of $Cu_6Sn_5$, it is prepared as active material, and there is no observation engaged with severe material detachment from carbon fabric during cycling. As a result, negative electrode which shows specific capacity about 300 mA h $g^{-1}$ stably could be made. When comparing with conventional negative electrode which uses Cu foil as a current collector, the specific capacity considering the weight of current collector is almost 70 % larger. The other beneficial feature offered by the carbon fabric current collector is negligible electrode swelling, which is possible because the void spaces in the carbon fabric can accommodate the volume expansion of $Cu_6Sn_5$ component.

The simple method for loading active material is invented to generalize the utility of carbon fabric. The conventional slurry spreading method is modified and applied to carbon fabric system. The viscosity of prepared slurry was decreased, and the slurry was soaked into carbon

fabric by home-made suction equipment. The solid content of prepared slurry was 30 *wt.* %, and the suction process was conducted during 3 mins. As a result, the weight of loaded slurry was about 1.8 times heavier than that of carbon fabric. From the thickness information, it is checked that the loaded slurry was almost penetrated into carbon fabric. The fabricated electrode shows a good electrochemical properties, and especially, it delivers the high volumetric capacity because of the loaded slurry, which fills the void spaces of carbon fabric.

$TiO_2$-deposited SUS fabric is prepared successfully to develop the flexible negative electrode. SUS fabric characterized by 3-dimensional structure is used as a current collector for negative electrode of lithium-ion battery. $TiO_2$ which plays the role of active material is deposited onto SUS fabric by liquid-phase deposition in the microstructure of core (SUS fabric, current collector)/shell ($TiO_2$, active material). The flexibility of $TiO_2$-deposited SUS fabric is tested under the extreme condition, called folding test, and there is no detachment of active material. When using $TiO_2$-deposited SUS fabric as negative electrode and executing folding test during electrochemical cycling, there is no change in voltage profile and the cycle performance compared with non-folded one. The reason for granted flexibility of $TiO_2$-deposited SUS fabric is summarized as follows. First, imposed stress occurred during flexible test is effectively dissipated by 3-dimensional structure of SUS fabric utilized as a current collector. Second, the stress experienced by active material is overcome with strong adhesion strength obtained via covalent bond between $TiO_2$ and SUS fabric generated during liquid-phase deposition. Third, the selection of active material, which undergoes less volume change during cycling, helps initial adhesion strength remain even after electrochemical cycling.

SUS fabric, which provides a 3-dimensionally well-constructed electric path and large contact area between active material and electrolyte, is utilized as a current collector for the high rate capable negative electrode. When comparing with the conventionally prepared negative electrode, which uses Cu foil as a current collector, they have a big difference in the structure of

current collector. As a result, the electrode composed by SUS fabric shows a better rate capability than the conventional electrode, although they use same kind of active material.

In this research, properties of negative electrode are improved by using unique current collector, although there is no modification in active material. There has been no sufficient research on current collector. However, the importance of current collector is now obvious, and it is expected for lots of following researches.

Keywords: lithium-ion batteries (LIBs), current collector, carbon fabric, SUS fabric, $Cu_6Sn_5$ alloy, $TiO_2$, liquid-phase depositioin, high capacity negative electrode, flexible negative electrode.

Student number: 2011-22933

# Contents

# List of Figures

# List of Tables

# Chapter 1. INTRODUCTION

## 1.1. Present situation of energy storage devices

With enormous interest in portable electric apparatus, energy storage devices have been researched briskly. Among them, lithium-ion batteries (LIBs) show superior properties, such as high energy density, long cycle life, eco friendliness and economical efficiency, and these properties makes LIBs the most popular energy storage device [1-4]. LIBs have already been successfully used in mobile phone, and the market size is now expanded into hybrid electric vehicle (HEV) and electric vehicle (EV) [5, 6]. It is attributed to the increasing importance of eco-friend energy sources and the regulation on fossil fuel. Thus, LIBs must be researched more, which can store the bigger energy and satisfy the regulation on energy usage.

Several properties are required to LIBs, depending on the kind of portable electric apparatus to which they are applied. For instance, to be used in EV as power supply, LIBs must show high power capability [7-9]. Furthermore, LIBs must present high capacity, because the driving distance relies on the capacity and the space is restricted on which they can be placed [10-12]. In the case of mobile phone, LIBs must show the great reversibility over the broad depth of discharge. In these days, there are up-coming markets for LIBs, such as wearable electronics [13-15]. For successful application, LIBs must resist the external stress, which can be imposed during charge/discharge, to be worn on one's person.

## 1.2. Properties of lithium-ion batteries

### 1.2.1. Development of lithium-ion batteries

Since Volta discovered the electromotive force, which makes the electronic flow between metals of different kind from each other, many types of modern batteries have been developed, and batteries are now researched as core device in electric apparatus.

Usually, electromotive force between negative electrode and positive electrode must be huge to get high electric energy. Thus, lithium, whose standard reduction potential is the lowest in negative electrode material as -3.04 V (*vs.* $Li/Li^+$), has received great attention. Also, lithium has small atomic weight to deliver high specific capacity. However, it showed the critical problem in safety. Thus, it has been researched to overcome the safety issue since 1950s. It was really late research start, compared with lead acid batteries and Ni-Cd batteries, which were developed from the late $19^{th}$ century. The early stage of lithium batteries experienced the serious matter in dendritic growth of lithium during the electrochemical cycling, caused internal short and safety problem. Thus, the research was concentrated on primary batteries, and the research for secondary batteries was hampered by safety and reversibility issues [16-19]. Furthermore, the secondary lithium battery, firstly commercialized by Moly Energy (company, Canada) and composed by lithium anode and $MoS_2$ cathode, exploded by thermal runaway. Thus, the research for secondary lithium batteries became hard of restriction. This constraint has been gradually overcome by "Rocking Chair Batteries" (Figure 1) in which lithium ion migrates into anode and cathode alternatively, suggested by Armand [20, 21].

In 1990, Sony (company, Japan) successfully commercialized the secondary battery, composed by graphite anode and $LiCoO_2$ cathode. Sony named it for lithium-ion batteries (LIBs), and this nomination has been used officially. The success in Sony has encouraged the following research

for LIBs. Furthermore, there are a lot of research for beyond LIBs, such as a lithium-sulfur battery, lithium-air battery and all-solid-state battery to improve the capacity and safety of battery [22-26].

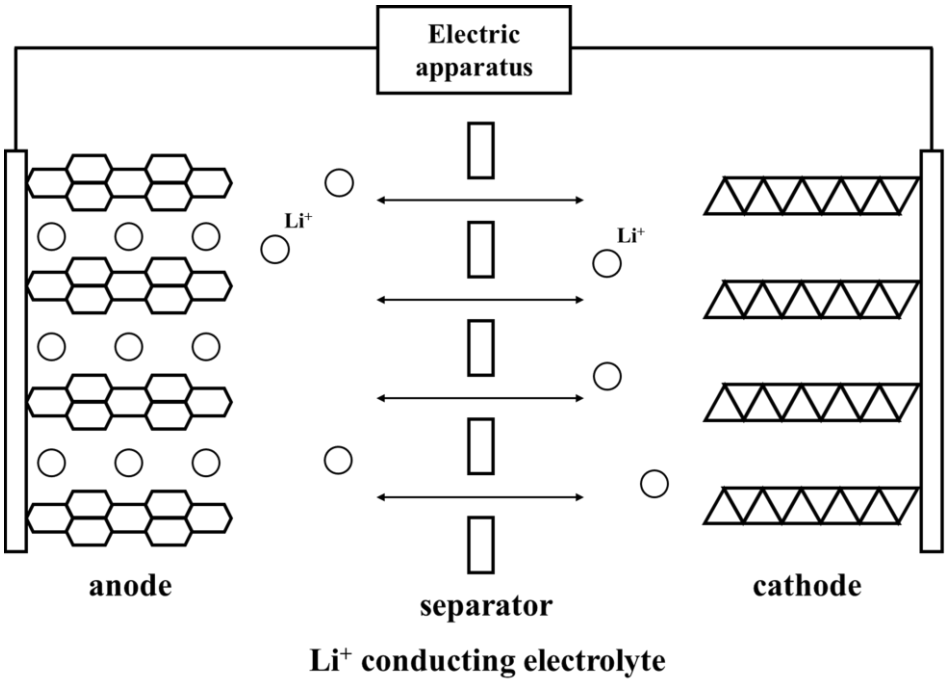


**Figure 1.** "Rocking chair batteries" in which lithium ion migrates into anode and cathode alternatively, suggested by Armand.

### 1.2.2. Principles of lithium-ion batteries

When the different kinds of metals, which have distinct electric potential, are linked together, electrons flow from the metal of higher electric potential to the metal of lower electric potential. The utilization of this electronic flow is the principle of batteries. Simultaneously, the migration of lithium-ion between anode and cathode is conducted through lithium-conducting electrolyte, and these phenomena must take place stably over the repeated electrochemical cycling. Cathode (positive electrode) is composed of lithium-inserted active material, and this lithium of cathode material transfers to anode (negative electrode) during charge. In the case of discharge, the lithium of anode material transfers to cathode again. The voltage of lithium-ion batteries is described as the electrochemical potential difference between lithium ion of anode and that of cathode. The commercialized LIBs are composed by graphite as anode whose electrochemical potential is about 0 ~ 1 V (*vs.* $Li/Li^+$) [27, 28] and lithium-containing metal oxide, such as $LiCoO_2$, $LiNiO_2$ and $LiMn_2O_4$, as cathode whose electrochemical potential reaches 4 V (*vs.* $Li/Li^+$) [29, 30]. Thus, the average voltage of commercialized LIBs is about 3.6 V, and it is such a high voltage, compared with the other energy storage devices.

## 1.3. Constitution of lithium-ion batteries

### 1.3.1. Components of batteries

Usually, LIBs are composed by many kinds of components, which must play the role exactly to operate well the battery as intended. There are four primary components, such as anode, cathode, electrolyte and separator (Figure 1). Beside these basic components, various ornaments are used to grant additional utilities to the battery.

Electrode plays the role as mediator which stores the electric energy in the form of chemical energy and utilizes the electric energy by transformation of chemical energy. Electrode consists of anode and cathode, and the electric potential of anode is lower than that of cathode. The electric potential difference between anode and cathode is expressed as voltage of the battery. In the case of charging, electrons flow from external electric circuit to anode, and lithium ion is inserted into anode from electrolyte simultaneously. Vice versa, when the battery is discharged, electrons flow from anode to external electric circuit, and lithium ion is extracted from anode to electrolyte.

Electrolyte helps the flow of lithium ion between the electrodes, and it must be an insulator to inhibit the transfer of electron. LIBs operate in the broad range of potential, compared with the other energy storage devices [18, 31]. To be stable in this condition, organic solvent is used, and the proper amount of lithium salt is dissolved into organic solvent to grant the ability of lithium transfer. Recently, aqueous electrolyte was researched by Kang Xu, and it was reported that the stability of aqueous electrolyte is incredibly improved by increasing the salt concentration [32].

Separator prevents the physical contact of the electrodes, and makes the electron flow be possible only by external electric circuit. It helps the electric energy to be used as intended. Separator is porous barrier, and during the electrochemical cycling, it is permeated by electrolyte to transfer lithium ion between the electrodes [33]. It should be electrochemically and chemically stable over long cycle life. Lately, the batteries developed by Samsung SDI (company, Korea) caught fire, and it was suspected that the reason is engaged with faulty of separator. Like this, separator is important component of LIBs for safety issue.

### 1.3.2. Components of electrodes

Looking at in more detail, electrode is also composed by several components. The components

are active material, binder, conducting agent and current collector. The electrode can be separated into two layers. One is the layer, in which active material, binder and conducting agent are uniformly mixed in the weight ratio of 90 : 5 : 5, and, it is placed onto the other layer, which is current collector (Figure 2).

Electric energy is stored as chemical energy of active material. Active material has the ability of storing lithium ion. Because of its importance, the research has been concentrated on active material. The new kind of active material, which shows a large specific capacity or high rate capability, has been explored. Also, the morphology of active material has been modified to be stabilized during the electrochemical cycling. Finally, surface modification of active material has been tried to transfer lithium-ion or electron rapidly, or to inhibit the electrolytic decomposition at surface.

Binder helps the other components be attached firmly onto current collector. For this reason, polymer, whose adhesion strength is high, is used as a binder [34, 35]. During the electrochemical cycling, active material experiences the volume change, and it causes fatigue accumulation, resulting in detachment of active material from current collector. And, in the case of wearable electronics, the LIBs can undergo external stress, which is imposed onto active material during daily use. Because of the stress, active material can be detached from current collector. These problems can be overcome by using the improved binder which has strong adhesion strength.

Electronic flow among active material is facilitated by conducting agent. The active material, like graphite and metal, has a superior electric conductivity, and there is no great needs for conducting agent. However, in the case of metal oxides, it has a deficient electric conductivity. When these low electric conductivity material are used as active material, the LIBs cannot show a sufficient rate capability to be commercialized. Thus, carbonaceous material, which has good electric conductivity and nano-size to be easily located among active material, is used as conducting

agent. Decomposition of electrolyte upon conducting agent can occur over the repeated electrochemical cycling. Thus, the method for inhibition of electrolytic decomposition upon conducting agent must be researched.

Current collector acts as a passage of electron between active material and external electric circuit. It should not be lithium-inserted or dissolved at the operated voltage range, and it must have a sufficient electric conductivity. The commercialized LIBs utilizes 2D copper foil as a current collector of anode and 2D aluminum foil as a current collector of cathode.

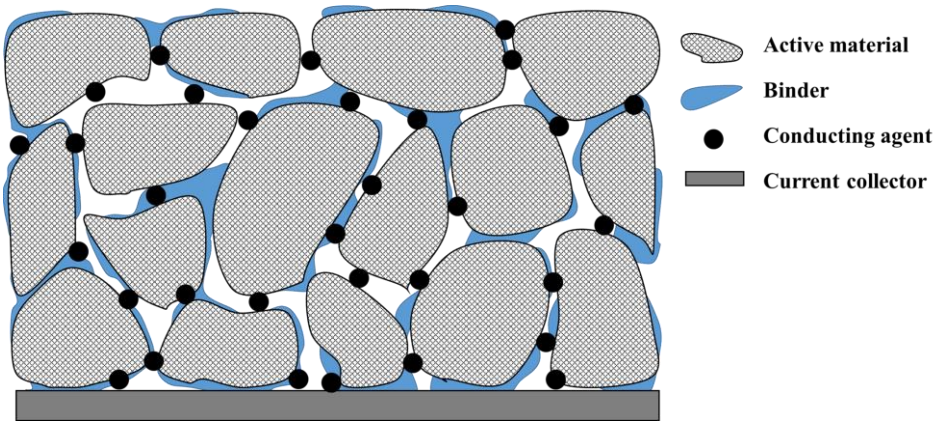


**Figure 2.** Basic design for electrode components of lithium-ion batteries.

## 1.4. Materials in negative electrode

To be used as an active material in negative electrode, there are several requirements to be satisfied. First, the standard reduction potential of active material must be similar with that of lithium metal. Then, the specific capacity of active material should be high, and it has to show stable cycleability over long cycle life. Also, it must present excellent rate capability, and safety issues should be overcome. In following section, various kinds of active material are introduced.

### 1.4.1. Metallic lithium

Lithium metal delivers the specific capacity of 3860 mA h $g^{-1}$ which is the highest value among active materials of anode (silicon is an exception). However, the critical problems must be overcome to use lithium metal in the commercialized LIBs. First, the standard reduction potential of lithium metal is too low to trigger the electrolytic decomposition onto surface of lithium [36]. It results in depletion of electrolyte and low Coulombic efficiency over the repeated electrochemical cycling. Also, during the repeated electrochemical cycling, dendritic lithium can grow from anode to cathode, penetrating the separator, to directly contact the electrodes [37, 38]. If things come to this stage, internal shortage takes place, which results in the serious problem, like catching fire. To solve the problems, lithium powder, which shows a large surface area, has been used as anode material [39]. Also, it is tried to increase the safety of LIBs by using solid-state electrolyte [40, 41].

### 1.4.2. Carbonaceous materials

In the case of commercialized LIBs, it uses carbonaceous materials as anode material. Carbonaceous materials are categorized into graphitic carbon and non-graphitic carbon.

Graphitic carbon presents the specific capacity of 372 mA h $g^{-1}$, and shows the reaction plateau at the similar voltage range with lithium metal. In graphitic carbon, graphene layers, which have honey-comb structure, are piled up as AB stacking, and lithium is inserted between them. Non-graphitic carbon shows the higher reversible specific capacity than graphitic carbon, and the voltage profile is drawn as slope. Lithium insertion in non-graphitic carbon is conducted not only between stacks but at edge or in cavity [42]. Thus, the various kinds of space for lithium storage increases the reversible specific capacity of non-graphitic carbon. However, non-graphitic carbon shows the lower Coulombic efficiency than graphitic carbon. Also, because the average reaction voltage of non-graphitic carbon is higher than that of graphitic carbon, the real energy density of non-graphitic carbon is not different from that of graphitic carbon, as expected by the difference of specific capacity.

### 1.4.3. Lithium-alloys

Carbonaceous materials shows stable cycleability over long cycle life, but it delivers the deficient specific capacity, for example, to meet the driving distance of electric vehicles as energy storage device. To solve this problem, the various kinds of active materials have been searched. Among them, tin (Sn) and silicon (Si) have attracted considerable attention [43, 44]. It is known that they receive 4.4 lithium atoms per each atom at the fully lithiated state ($Li_{4.4}Sn$ and $Li_{4.4}Si$), and, in this case, the specific capacity of tin and silicon reaches 998 mA h $g_{Sn}^{-1}$ and 4200 mA h $g_{Si}^{-1}$, each. Recently, it was reported that the maximum number of lithium atom, which tin and silicon can receive during lithiation, is modified to 3.5 [45]. In the case of tin, it presents the smaller specific capacity than silicon. However, the electric conductivity of tin is higher than that of silicon to show high rate capability, and the volumetric capacity of tin is similar with that of silicon. Lithium-alloys usually deliver the high specific capacity, but experiences large volume change

during the electrochemical cycling. Both materials, tin and silicon, expand in the degree of 250 ~ 300 % in the state of fully lithiated [43], and it is much higher than that of graphite, which undergoes the volume expansion in the degree of 10 % in fully lithiated state [46]. During the repeated volume change, cracks are generated on the surface of active material, resulted in additional electrolytic decomposition onto the newly exposed surface. In this process, Coulombic efficiency is consistently low. Also, additional electrolytic decomposition thickens the solid-electrolyte interphase (SEI), and dead particles, which is inactive with lithium ion, are formed [47]. Many researches have been done to resolve the problems engaged with dead particles (capacity fading). First, nano-sized particles are used as active material, which scarcely experience crack generation on surface during the electrochemical cycling [48]. Secondly, lithium-inactive species, like copper, have been used to form intermetallic with tin and silicon [49, 50]. Intermetallic undergoes less volume change during the electrochemical cycling to show stable cycle retention. Lastly, additives in electrolyte, such as vinyl carbonate (VC) and fluoroethylene carbonate (FEC), have been utilized to generate stable SEI on the surface of active material [51, 52].

### 1.4.4. Metal oxides

The study for novel material of high specific capacity have discovered the various kinds of metal oxides, such as SnO, SiO, $Li_4Ti_5O_{12}$ and $TiO_2$. In this part, the explanation for $TiO_2$ is following. Active materials, like metallic lithium, carbonaceous material and lithium-alloy, have the problem engaged with electrolytic decomposition on the surface, because of their low standard reduction potential. To overcome the problem, the active materials, which shows the high reduction potential and undergoes no electrolytic decomposition, have been researched, like $TiO_2$ [53]. It shows the reaction plateau at 1.8 V (*vs.* $Li/Li^+$), and experiences no volume change during

the electrochemical cycling to show stable cycle retention. Also, there is no electrolytic decomposition to present excellent Coulombic efficiency. However, $TiO_2$ delivers the low specific capacity, compared with the commercialized graphitic carbon, and it shows the poor rate capability, because of its low electric conductivity. Nevertheless, when it comes to the field of wearable electronics, $TiO_2$ is a good candidate for anode material. Although the material does not experience volume change during the electrochemical cycling, solid-electrolyte interface (SEI) can be damaged to cause additional electrolytic decomposition by the external stress, which is imposed during daily use, such as bending and folding. In this operating condition, active material, which has the operating voltage range of electrolyte being stable, must be used, and $TiO_2$ meets the requirement.

## 1.5. Characteristics in this work

As mentioned before, Cu foil and Al foil are conventional current collectors in lithium-ion batteries. Cu foil is the current collector for negative electrode, and Al foil is the current collector for positive electrode. In this work, we escape from the specified framework on the use of current collector and adopt novel kinds of current collectors to develop desirable electrodes.

Novel kinds of current collectors could be categorized as follows. Firstly, the materially unique current collector can be suggested to fabricate the electrode of lithium-ion batteries. In this work, graphite and stainless steel (SUS) are utilized as candidates of current collector. All the kinds of suggested material shows a sufficient electric conductivity to be utilized as a current collector. Especially, carbon shows a reactivity with lithium ion at the voltage range of conventional negative electrodes. Thus, when carbon material is used as a current collector to fabricate the negative electrode, it delivers the higher capacity than the conventionally prepared negative electrode.

Secondly, the structurally unique current collector can be suggested to fabricate the electrode of lithium-ion batteries. The structure of electrode is determined by the structure of current collector. In this work, fabric is adopted as a structure of current collector. This structure is well-known to relive the imposed stress onto electrode during daily use by distributing the stress effectively. Thus, flexible electrode can be developed by adopting the fabric current collector to fabricate the electrode. Also, 3-dimensionlly well-constructed electric network can be obtained from fabric structured current collector. Thus, it is possible to develop the high rate capable electrode.

# Chapter 2. EXPERIMENTAL

## 2.1. Synthetic procedures

### 2.1.1. $Cu_6Sn_5$-deposited carbon fabric

Cu and Sn were deposited on a carbon fabric (JNTG Co., Korea) by using electro-less plating technique. The Cu electro-less plating was performed at 60 $^oC$ for 120 s in MID Copper 100 bath (MacDermid Company, Korea), which was followed by Sn electro-less plating at 60 $^oC$ for 180 s in YL-Tin bath (YuLim T&C, Korea). After the two consecutive electro-less platings, the carbon fabric was thoroughly washed with distilled water and dried at 80 $^oC$ for 20 min. Then, the carbon fabric was heat-treated at 400 $^oC$ for 10 h in argon atmosphere to obtain the $Cu_6Sn_5$-deposited carbon fabric electrode [54]. As a comparison purpose, the conventional-type electrode was prepared. To this end, $Cu_6Sn_5$ powder was synthesized by mixing Cu and Sn powder in the stoichiometric ratio, and heat-treating at 400 $^oC$ in argon atmosphere for 10 h. The resulting $Cu_6Sn_5$ powder was mixed with a conductive carbon (Super-P), styrene-butadiene rubber (SBR) and carboxymethyl cellulose (CMC) (85:5:5:5 in *wt.* %) and dispersed in water. The resulting slurry was spread onto a piece of Cu foil and dried at 120 $^oC$ for 10 h under vacuum. Experimental scheme is summarized as Figure 3.

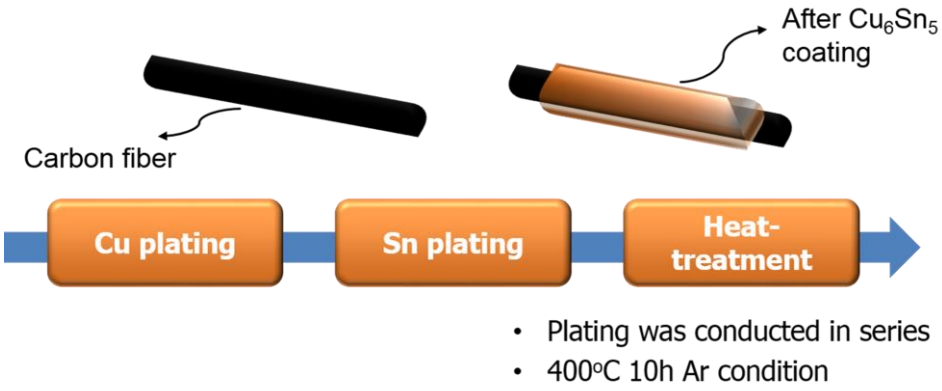


**Figure 3.** Experimental scheme for $Cu_6Sn_5$ deposition on carbon fiber paper (carbon fabric)

### 2.1.2. $TiO_2$-deposited SUS fabric

SUS fabric (Orangepower, Korea) was used as received. It is composed of SUS fiber and shows free-standing properties, which makes it possible to be utilized as a current collector directly. There are a lot of void spaces at the inside of fabric, and the thickness of SUS fabric amounted to about 80 μm. $TiO_2$ deposition on SUS fabric was conducted as follows. First, piranha solution was prepared by mixing 35 ml sulfuric acid (98 *wt.* %, DAEJUNG) with 15 ml hydrogen peroxide (30 *wt.* %, DAEJUNG) slowly at room temperature. Then, the piece of SUS fabric (3cm * 4cm) was dipped into piranha solution for 20 minutes to form hydroxyl group on the surface, and the temperature of bath was maintained at 80 $^{o}$C [55]. Second, 0.06 *M* $(NH_4)_2TiF_6$ (Alfa aesar) of 50 ml and 0.18 *M* $H_3BO_3$ (Sigma Aldrich) of 50 ml was made and mixed to prepare the bath for liquid-phase deposition. After SUS fabric treated by piranha solution was sonicated in distilled water for 10 minutes, it was placed vertically in deposition bath for 3 h, and the temperature was maintained at 80 $^{o}$C. The above process was repeated twice more, using newly prepared deposition bath. In the repeated process of deposition, the thickness of $TiO_2$ on SUS fabric became thicker. After the termination of deposition, the deposited SUS fabric was dried at room temperature for 1 day. Then, the deposited SUS fabric was heat-treated at 500 $^{o}$C for 5 h in air condition. During the heat-treatment, the phase of deposit was stabilized and the impurities engaged with fluorine was replaced by oxygen. The experimental process is summarized as Figure 4. At the bottom of deposition bath, there are a lot of precipitated powder, which has similar properties with deposit on SUS fabric. Thus, the powder was recollected and examined to infer the phase and morphology of deposit.

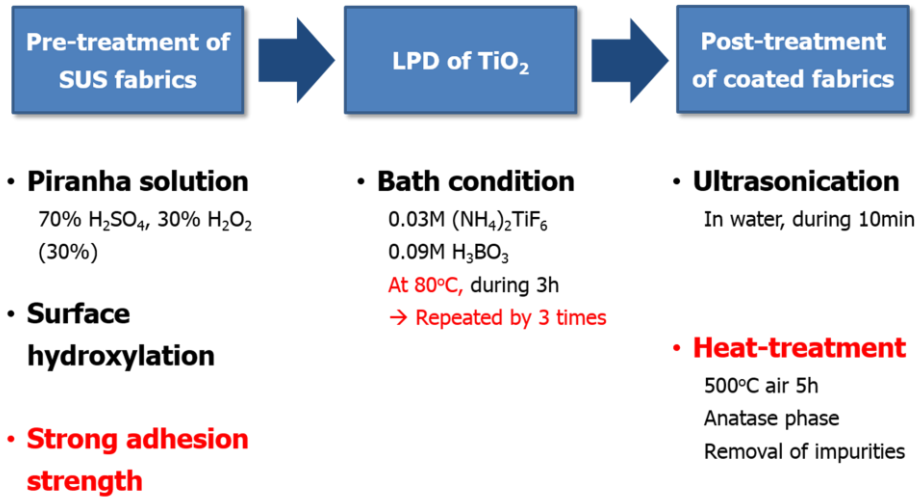


**Figure 4.** Experimental process for $TiO_2$ deposition on SUS fabric.

## 2.2. Electrochemical test condition

Two-electrode coin cells (CR2032) were assembled with lithium metal foil and poly propylene (PP)-poly ethylene (PE)-PP separator. The used electrolyte was 1.0 *M* $LiPF_6$ dissolved in a mixture of ethylene carbonate (EC) and diethyl carbonate (DEC) (1:1 in *vol.* ratio).

### 2.2.1. Cycling condition for $Cu_6Sn_5$-deposited carbon fabric electrode

The charge/discharge cycling was carried out by means of a constant current–constant voltage mode for lithiation, in which the current was fixed at 0.2 *C*-rate until the potential dropped to 20 mV (*vs.* $Li/Li^+$) and then the potential was held at 20 mV (*vs.* $Li/Li^+$) until the current dropped to 0.05 *C*-rate. The de-lithiation was performed in a constant current mode at 0.2 *C*-rate to 1.2 V (*vs.* $Li/Li^+$). The *C*-rate was calculated on the basis of the reversible specific capacity delivered by the two Li-active components; 457 mA h $g^{-1}$ by $Cu_6Sn_5$ and 200 mA h $g^{-1}$ by carbon fabric. The galvanostatic intermittent titration technique (GITT) was employed to monitor the thermodynamic voltage profile, in which a current pulse was applied to measure the closed circuit voltage (CCV) and turned off to obtain the quasi-open circuit voltage (QOCV).

### 2.2.2. Cycling condition for $TiO_2$-deposited SUS fabric electrode

The electrochemical cycling was carried out by means of a constant current mode for lithiation, in which the current was fixed at 0.1 *C* (coin-type) or 0.2 *C* (pouch-type) until the potential dropped to 1.5 V (*vs.* $Li/Li^+$). The de-lithiation was performed in a constant-current mode at 0.1 *C* (coin-type) or 0.2 *C* (pouch-type) to 2.5 V (*vs.* $Li/Li^+$).

### 2.2.3. Electrochemical analysis methods

To confirm properties of the prepared active material, various experimental tools are developed and applied. Scanning electron microscope (SEM) and transmission electron microscope (TEM) are used to check the morphology of material. X-ray diffractometer (XRD) is utilized to confirm the phase of material. To assure the surface information of material, X-ray photoelectron spectroscope (XPS) is used. In this work, research concentrates on developing superior negative electrodes. Thus, it is comfortable to characterize the properties by electrochemical analysis tools. Simply, by the electrochemical cycling, we can know how much the capacity and how stable the cycle retention. Furthermore, the other electrochemical analysis tools help us understand the traits of materials.

#### 2.2.3.1. Differential capacity (dQ/dV) plot

Looking into the voltage profile of crystallized material, reaction plateau is well developed. The potential of reaction plateau depends on the kinds of active material. Thus, the kinds of active material can be inferred by the potential of reaction plateau. However, the exact potential cannot be detected only by voltage profile. Instead, when the voltage profile is processed by mathematical method, the information about potential can be easily seen. The differential capacity plot makes the potential of reaction plateau outstand.

#### 2.2.3.2. Galvanostatic intermittent titration technique (GITT)

The standard reduction potential of active material is decided by thermodynamic property of the material. However, the real voltage profile, obtained during the electrochemical cycling, is different from the profile, anticipated by the thermodynamic information. The reason for

disagreement between real data and thermodynamic data is overpotential, and it has an influence on rate capability and energy efficiency of the batteries. To grasp the extent of overpotential, GITT method is applied in many cases [56]. GITT method tells the overpotential of material at the reaction range by detecting the difference between closed circuit voltage (CCV) and quasi-open circuit voltage (QOCV). During experiment, a current pulse was applied to measure CCV and turned off to obtain QOCV (Figure 5). In the case of lithium-alloying material, which experiences large volume change, it was reported by GITT method that the large overpotential is exerted at fully discharged state [57]. Also, the overpotential at lots of cycling number can be easily analyzed by GITT method.

#### 2.2.3.3. Electrochemical voltage spectroscopy (EVS)

Various electrochemical methods are invented to understand thermodynamic information of active material. Among them, EVS is the most effective analysis method in the aspect of saving time. Also, EVS method tells the maximum capacity of the material quickly [58]. By inspecting the current decay shape during constant voltage mode, the mechanism of reaction with lithium can be illuminated (Figure 6).

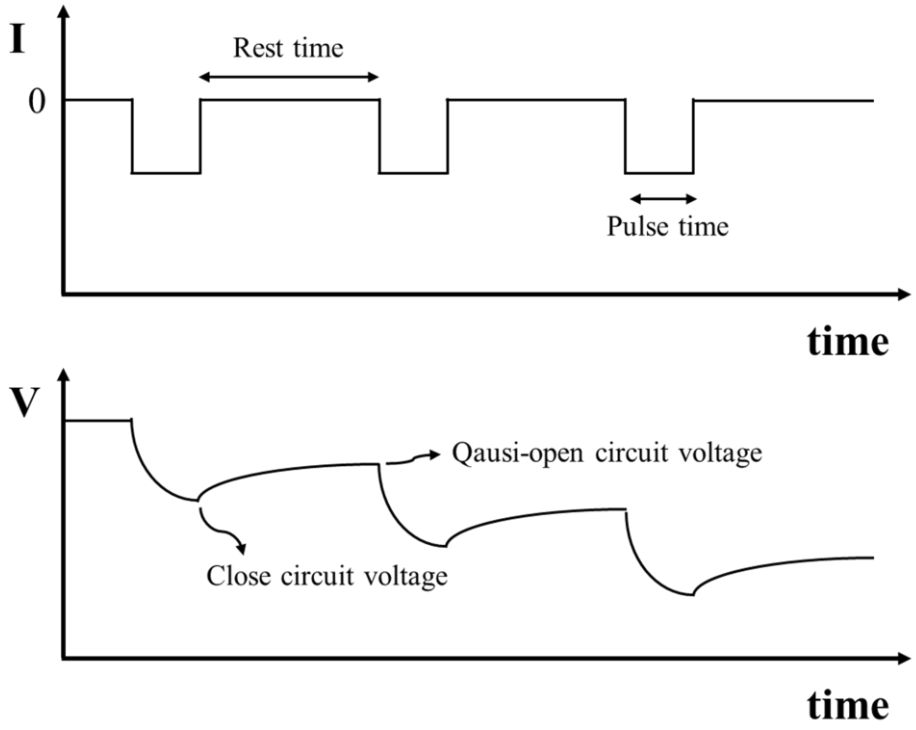


**Figure 5.** Schematic diagram of galvanostatic intermittent titration technique.

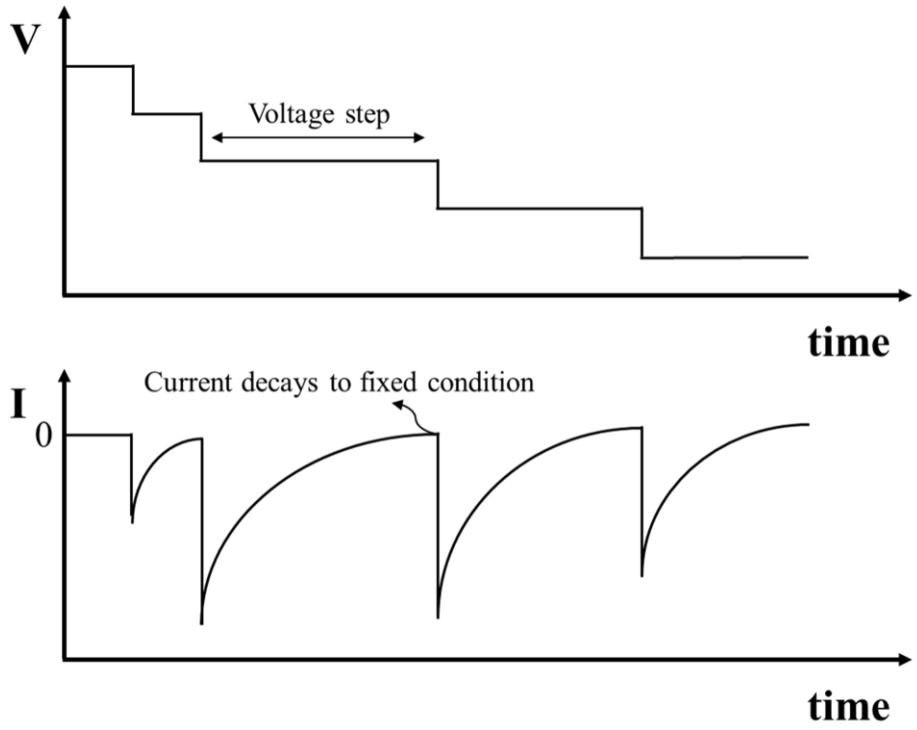


**Figure 6.** Schematic diagram of electrochemical voltage spectroscopy.

## 2.3. Material characterization

The electrode morphology was examined by using a field-emission scanning electron microscope (FE-SEM, JSM-6700F). To obtain the cross-sectional images, the electrode samples were crosscut by using an argon-ion beam polisher (JSM-09010) at a constant power of 0.5 W (5 kV and 0.1 mA) under vacuum (<$2.0*10^{-4}$ Pa). The X-ray diffraction (XRD) patterns were obtained by using a D8-Bruker diffractometer equipped with Cu Kα radiation (1.54056 Å). The XRD patterns were recorded at 40 kV and 40 mA using a continuous scanning mode with 5.0 degree $min^{-1}$. The thickness change of electrode was traced by using a micrometer. The morphology of powder was checked by utilizing a trans-mission electron microscopy (TEM, JEM-3010). The phase of powder was examined by Raman microscopy (T64000). The chemical composition of surface on the electrode was analyzed by using an X-ray photoelectron spectroscopy (XPS). Al Kα (1486.6 eV) radiation was used at 100 W (15 kV and 10 mA). The binding energy was calibrated by the C 1s peak of hydrocarbon (285.0 eV). For the peel test, a piece of electrode was attached to 3M adhesive tape, and its peel strength was measured with a micro material tester (JSV H1000). All the electrodes were prepared as a shape of 10 mm wide and 60 mm long, and the speed of displacement was 30 mm $min^{-1}$ during peel test.

# Chapter 3. RESULT AND DISCUSSION

## 3.1. High capacity negative electrode by using lithium-active and light-weight carbon fabric as a current collector

### 3.1.1. Strategies for high capacity negative electrode

Many devices from information technology apparatus to electric vehicles (EV) have utilized electric energy. Therefore, it becomes more and more important to keep electric energy stable. Among a great number of candidates, lithium-ion batteries (LIBs) are the best selection for many reasons [59]. LIBs show a larger capacity and higher power capability than other energy storage appliances. Thus, LIBs are promising candidates and there has been many attempts to make it better [44, 60-63]. However, advanced LIB with lager capacity than currently achievable one should be developed to meet the requirements of EV [64].

The strategy for developing large capacity LIB has been mainly focused on the search for novel active material. For example, silicon and tin have been researched a lot as active material for negative electrode [49, 60]. When compared with commercialized one, graphite, these materials show much larger capacity. However, they have intrinsic problems such as severe volume change during cycling. Mostly, novel material known to have high capacity shows poor cycleability, and it is hard to develop desirable electrode which exhibits not only high capacity

but stable cycleability [57]. Therefore, it is tried to develop large capacity negative electrode through different approach with conventional strategy, for example, by changing the amount or characteristics of electrode component.

Electrode is mainly composed of active material, conducting agent, binder and current collector. Among them, active material is only component which has reactivity with lithium ion to deliver capacity. Therefore, it is possible to increase capacity of electrode by decreasing the amount or modifying the characteristic of lithium non-active component. In this study, conducting agent and binder is not used in electrode fabrication process, and more importantly the trait of current collector is modified to develop desirable negative electrode.

Carbon is a good electric conductor to holds qualification as a current collector. Additionally, carbon is reactive with lithium ion at the potential window of negative electrode [28, 65, 66]. Thus, the attempt to use carbon as a current collector can be very effective in the aspect of the specific capacity. To use carbon as a current collector, the structure of carbon is important. When active material is deposited on current collector of conventional structure, the reactivity with lithium ion is greatly hindered, because the thick layer of active material must come into large polarization. Therefore, fabric structure is used to increase the surface area of electrode. Because of its large surface area, the thickness of active material deposited onto fabric can be considerably diminished. In addition, lithium ion transfer between active material and electrolyte becomes easy by virtue of large surface area. Consequentially, the problem engaged with reactivity of carbon current collector can be overcome.

The traits of carbon fabric leads to several advantages as a current collector. Above all, it is not only light but active with lithium ion. In conventional system, copper foil is used as a current collector, and it is non-active with lithium ion as well as heavy. Therefore, as carbon fabric replaces the copper foil, it can expand the specific capacity of overall electrode greatly compared with conventional system. Also, there are many empty spaces among fibers. These empty spaces

could be very useful during cycling [63, 67-69]. Almost of active material experiences volume change during cycling, and it induces the change in overall thickness of negative electrode. Considering the actual battery configuration, thickness increase in electrode puts battery into a dangerous state. The battery could be swelled, and also the package of battery could be damaged. In this situation, cavities could reduce overall thickness change during cycling by accommodating the volume change and raise the safety of battery. However, these empty spaces could be a weak point in the aspect of volumetric capacity simultaneously.

There are several candidates for active material, for example, tin and copper–tin alloy. Although tin has large theoretical capacity and adequate for electroplating, it has intrinsic problem engaged with cycleability. In this study, electrode is composed of active material and current collector only. In binder-free system, active material loss might happen easily during cycling which results in capacity fading [35, 70, 71]. Therefore, copper-tin alloy is selected as active material. Cu acts a role as buffer matrix, and prevents the detachment of active material from current collector during cycling [49, 50].

In this research, carbon (core) – $Cu_6Sn_5$ (shell) fabric electrode was successfully prepared. Because current collector (carbon fabric) is also reactive with lithium ion, composite fabric electrode can show high specific capacity when considering the weight of whole electrode components. When utilizing current collector which has porous structure, it could make several advantages in battery performance related with rate capability and volume change. These traits induced by structural characteristics were compared with conventional system which uses Cu foil as a current collector.

### 3.1.2. Characterization of deposited carbon fabric

The morphology of electrodes are confirmed by Figure 7. Figure 7a is the optical image of

current collector (carbon fabric). It is checked that carbon fabric is free-standing and this fabric can be directly used as a current collector. There are FE-SEM images of current collector through Figure 7b-c. There are a lot of carbon fibers and these fibers are stick together firmly. Carbon fabric is not only composed by carbon fibers but carbon particles (inner circle of Figure 7b). The role of carbon particles is to fix fibers each other. According to JNTG Company, the fabrication method of carbon fabric was explained as follows. First, chopped carbon fiber was well mixed with polymer resin. In this step, the phase of carbon fiber was graphite already, and the compound was stick together by polymer resin. Then, the compound was heated to make polymer resin carbonized. In this process, polymer resin became carbon particles. The diameter of carbon fiber is about 7 μm, and the surface is smooth.

There are images of $Cu_6Sn_5$-deposited carbon fabric electrode through Figure 7d-f. Uniform deposition can be confirmed by images of low magnification (Figure 7d). As seen in the magnified images (Figure 7e), morphology of surface is different with that of carbon fabric. When preparing $Cu_6Sn_5$ alloy as active material, the surface of electrode becomes rough. More specifically, according to FE-SEM images of the sample processed by cross-sectional polisher (Figure 7f), uniform deposition along radial direction can be checked, and the thickness of $Cu_6Sn_5$ is about 1 μm. It allows us to infer that carbon fiber locates in the inner part (core material) and $Cu_6Sn_5$ locates in the outer part (shell material). Also, because there is a lot of cavities among fibers, it is helpful for active material to expand during lithiation. It could accommodate the internal stress to improve cycleability.

It is examined by XRD to check what phase constitutes the electrode (Figure 8). In the upper graph, the peak of graphite is shown well, and as seen in the magnified graph (inset), even the weak peaks of carbon fabric are well matched with that of graphite. The broad peak around 25 $^{o}$ is an evidence for presence of non-graphitized carbon. Thus, it allows us to conclude that the phase of carbon fabric is composed of graphite (carbon fiber) and non-graphitized carbon

(carbon particle). In the middle graph, there are several peaks of $Cu_6Sn_5$ plus the peak of graphite. There are also peaks engaged with metal oxide, like copper oxide and tin oxide, but the intensity of them is very weak. It is estimated that these phases are produced during heat-treatment process. Consequently, it is noted that main components of composite fabric electrode are graphite at core and $Cu_6Sn_5$ at shell respectively. In the lower graph, the diffraction peaks of synthesized powder is confirmed as $Cu_6Sn_5$ alloy.

GITT test was executed to examine the phase of carbon fabric by electrochemical test. The inset image of Figure 9a is GITT data of carbon fabric during lithiation. Current pulse was applied to measure the CCV and turned off to obtain the QOCV. When using QOCV data, the thermodynamic voltage profile could be obtained. As seen in Figure 9a, the staging phenomenon of graphite is checked well in carbon fabric. Furthermore, the differential capacity plot elucidates that the peaks are same with that of graphite in the aspect of type and position (Figure 9b) [58]. However, the specific capacity of carbon fabric is lower than ideal capacity of graphite. Carbon particles added to fix fibers together is thought to be the main reason for deficiency of capacity. Carbon particles is residue of polymer resin after carbonization process, and the heat-treatment temperature reaches about 1600 $^{o}$C which is not sufficient to make polymer resin graphitized. Namely, it is confirmed that the phase of carbon fiber is graphite by XRD experiment and differential capacity plot of QOCV, and the reason for capacity deficiency is carbon particle which grant the property of free-standing to current collector.

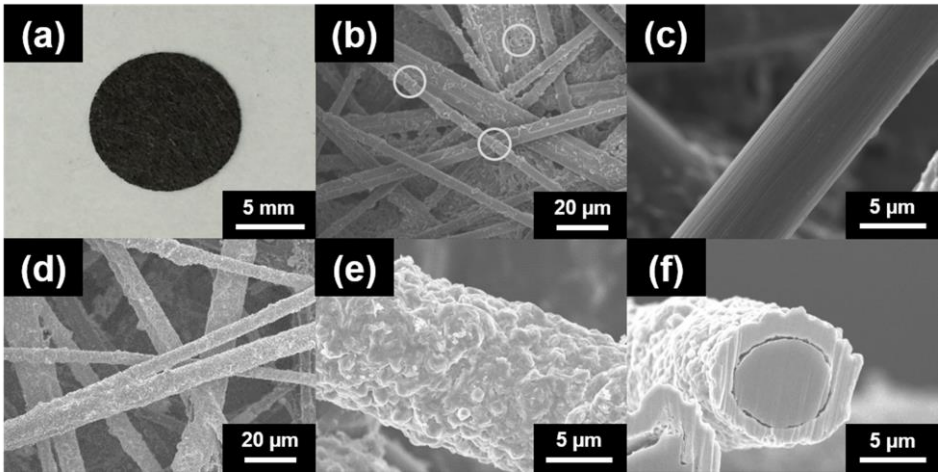


**Figure 7.** (a); The optical image of carbon fabric that was used as a current collector, (b) and (c); FE-SEM images of carbon fabric. (d) and (e); FE-SEM images of $Cu_6Sn_5$-deposited carbon fabric, and (f); cross-sectional FE-SEM image of $Cu_6Sn_5$-deposited carbon fabric. The circles in (b) indicate the binding carbons for the carbon fibers.

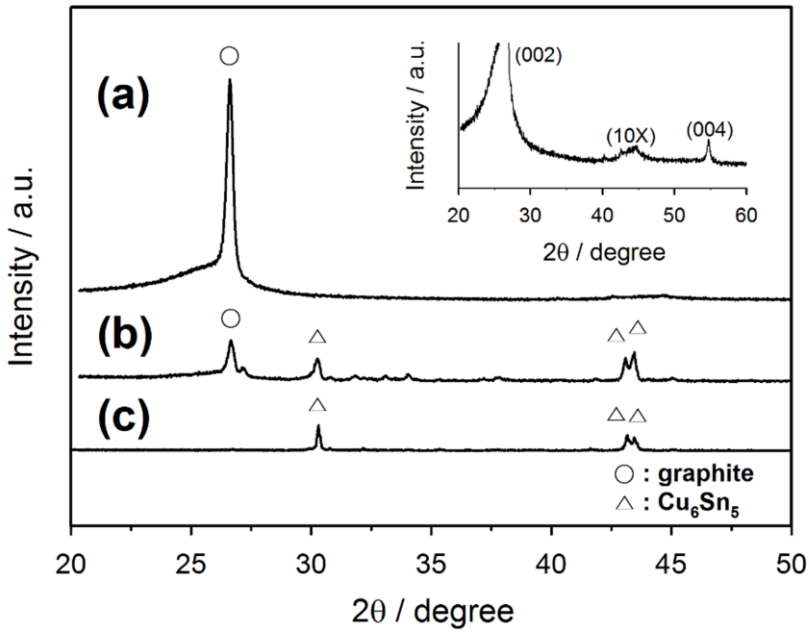


**Figure 8.** XRD patterns: (a); carbon fabric, (b); $Cu_6Sn_5$-deposited carbon fabric and (c); $Cu_6Sn_5$ powder. The magnified view of (a) is displayed in the inset.

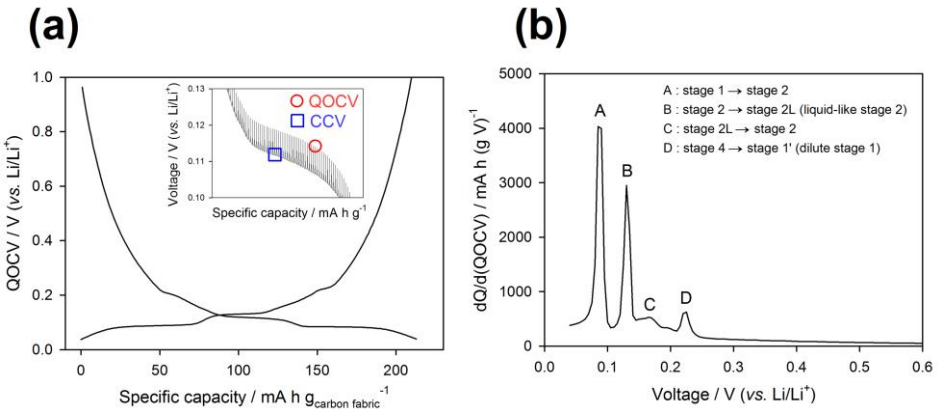


**Figure 9.** (a); The quasi-open-circuit voltage (QOCV) profile derived from the galvanostatic intermittent titration (GITT) data (inset) obtained from the Li/carbon fabric cell. (b); The differential capacity (dQ/dV) plot derived from the QOCV profile during de-lithiation shown in (a).

### 3.1.3. The comparison of $Cu_6Sn_5$-deposited carbon fabric electrode with the conventionally prepared $Cu_6Sn_5$-coated Cu foil electrode

The galvanostatic charge/discharge voltage profiles are compared for three electrodes in Figure 10a-c. The reversible specific capacity of $Cu_6Sn_5$-deposited carbon fabric electrode is about 288 mA h $g_{total}^{-1}$, and the areal capacity is 3 mA h $cm^{-2}$ in the first cycle. In this graph, capacity is divided by initial weight of all materials constituting negative electrode to consider the weight of current collector. The initial Coulombic efficiency of $Cu_6Sn_5$-deposited fabric electrode is somewhat low, because of metal oxides generated during heat-treatment. The copper oxides and tin oxides irreversibly react with lithium in the lithiation period. Compared with carbon fabric electrode (Figure 10c), the value for capacity is increased by introducing shell material which has higher specific capacity than graphite. The amount of increase is more dramatic in the aspect of areal capacity (1 mA h $cm^{-2}$ → 3 mA h $cm^{-2}$). Also, compared with $Cu_6Sn_5$-coated Cu foil electrode, the value for capacity is increased by using lithium-active current collector. The reversible specific capacity of the conventional-type electrode ($Cu_6Sn_5$-coated Cu foil) is 168 mA h $g^{-1}$ in the first cycle (Figure 10b). Note that the kind of active material is equal in the two electrodes, and there is only difference in lithium-inactive components (binder, conducting agent and current collector). Thus, it can concluded that the use in lithium active current collector increases the specific capacity greatly. In order to estimate the lithium storage capacity of carbon fabric itself, a carbon fabric electrode was fabricated and galvanostatically cycled (Figure 10c). The carbon fabric electrode delivers a specific capacity amounting to 200 mA h $g^{-1}$. Also, carbon fabric delivers about 1 mA h $cm^{-2}$, and cycleability is considerably stable. Therefore, it is possible to use carbon fabric as a current collector. In spite of previous data which allows us to infer that

the phase of carbon fabric is almost graphite, the staging phenomenon of graphite is not shown in voltage profile. It seems that the charge/discharge current is too high to confirm the thermodynamic data of carbon fabric. The capacity retention in the voltage cut-off range of 0.02~1.2 V is compared for the two cells in Figure 10d, in which the $Cu_6Sn_5$-deposited carbon fabric electrode exhibits a better capacity retention compared to the conventional-type electrode.

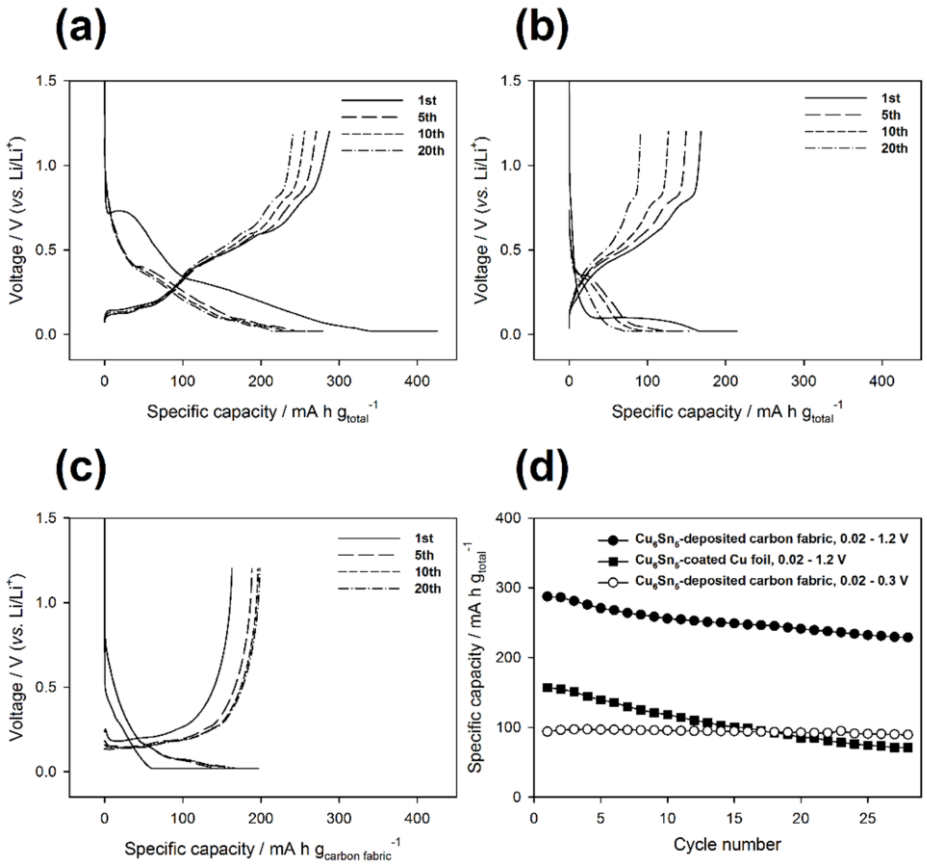


**Figure 10.** The charge (de-lithiation)/discharge (lithiation) voltage profiles obtained from: (a); Li/$Cu_6Sn_5$-deposited carbon fabric cell, (b); Li/$Cu_6Sn_5$-coated Cu foil cell, and (c); Li/carbon fabric cell. (d); Capacity retention for two cells. The voltage cut-off range is indicated in the inset. The specific capacity in (a) and (b) was calculated on the basis of the total weight of electrode ingredients including passive components.

It should be confirmed that core and shell material participate together to deliver capacity. Because shell layer is thick and dense, it could be hard for lithium ion to permeate through the outer layer and access core material. The reactivity of core material is checked by the differential capacity plot of composite fabric electrode (Figure 11a). When the cell is constructed by only using carbon fabric (current collector), there are several peaks under 0.3 V (*vs.* $Li/Li^+$), and it is characteristic peaks of graphite material. When using carbon core/$Cu_6Sn_5$ shell fabric electrode, there is no change in the kind of peaks below 0.3 V (*vs.* $Li/Li^+$) compared with carbon fabric, and there are additional peaks above 0.3 V (*vs.* $Li/Li^+$) aroused from shell material. Thus, it can be induced that the reactivity of core material is not hindered by shell material. Rather, when there is outer layer on carbon fabric, the polarization experienced by graphite seems to be smaller than that of carbon fabric only. It means that the reactivity of graphite with lithium ion is better in composite fabric electrode.

Also, to demonstrate the reactivity of core material with lithium ion, the ex-situ XRD experimental is conducted to observe phase transition (Figure 11b). In the case of carbon fabric (current collector), $LiC_6$ phase is detected well after 1$^{st}$ lithiation. Also, there is a weak peak assigned by $LiC_{12}$. It allows us to infer that the reactivity of carbon fabric with lithium ion is not sufficient during initial stage of cycling. Actually, areal capacity of carbon fabric is on the gradual increase from 1$^{st}$ to 10$^{th}$ cycle (Figure 10c). In the case of $Cu_6Sn_5$-deposited fabric electrode, the peak of $LiC_6$ phase is well shown, and the gradual increase of areal capacity is not observed (Figure 10d). Therefore, even though there is outer layer, it can be deduced that core material reacts well with lithium ion to present specific capacity.

As shown in Figure 11a, the lithiation/de-lthiation reaction takes place mainly below the 0.3 V (*vs.* $Li/Li^+$) for the core component (carbon fabric), whereas it takes place above the 0.3 V for the shell component ($Cu_6Sn_5$). $Cu_6Sn_5$-deposited carbon fabric electrode shows a moderate cycle retention when cycled in the voltage range of 0.02 ~ 1.2 V (Figure 10d). The cycle performance

of this electrode was also assessed in the voltage range of 0.02 ~ 0.3 V and presented in Figure 10d. As is seen, the cycle performance is excellent, which implies that the moderate cycle retention observed at 0.02 ~ 1.2 V is caused mainly by the capacity decay of the shell component ($Cu_6Sn_5$). This is not surprising if one considers the massive volume change of $Cu_6Sn_5$ upon cycling. The specific capacity observed at 0.02 ~ 0.3 V, which must be contributed by the core component, is about 97 mA h $g^{-1}$ on the basis of total electrode weight. The specific capacity shared by the core component, which was calculated considering the *wt.* % of carbon fabric in the core/shell electrode, is 186 mA h $g^{-1}$. This is comparable to the value observed with the carbon fabric electrode (Figure 10c). This illustrates that the core component delivers almost of its latent capacity even if the shell component is deposited on it.

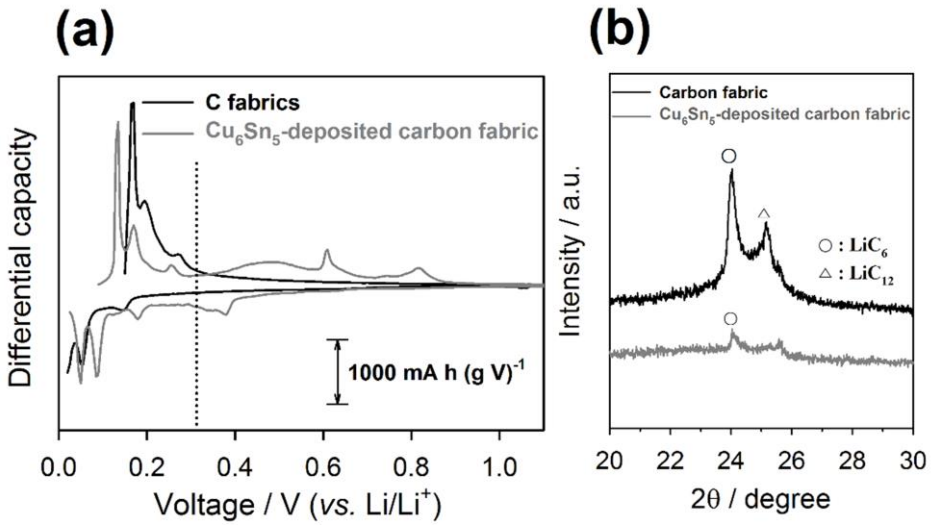


**Figure 11.** (a); The differential capacity (dQ/dV) plots derived from the galvanostatic voltage profiles obtained in the 6$^{th}$ cycle. (b); The *ex-situ* XRD patterns of two electrode samples.

**Table 1.** The comparison of areal capacity for two electrodes

| | **$Cu_6Sn_5$-deposited carbon fabric** | **$Cu_6Sn_5$-coated Cu foil** |
|---|---|---|
| Areal capacity (0.02 ~ 1.2 V) | 3.07 mA h $cm^{-2}$ | 1.05 mA h $cm^{-2}$ |
| Areal capacity (0.02 ~ 0.3 V) | 1.04 mA h $cm^{-2}$ | - |

It is possible to analysis the respective information of fabric electrode and conventional electrode on the basis of electrochemical data (Table 3). In the case of fabric electrode, the areal weight and the capacity of carbon fabric is known (Table 1). Also, those of $Cu_6Sn_5$-deposited fabric electrode is measured. Thus, the properties of shell material can be calculated. The calculated specific capacity of shell material ($Cu_6Sn_5$) is about 383 mA h $g^{-1}$, and it delivers similar capacity with previously reported. Therefore, it allows us to conclude that shell material delivers its capacity in like manner compared with $Cu_6Sn_5$ on conventional current collector. Then, calculation results of counterpart representing the conventional electrode is also filled in Table 1. It was assumed that the weight ratio of components are same between the fabric electrode and conventional electrode. The calculation of specific capacity of electrode is based on experimental data (381 mA h $g^{-1}$). As a results, the information of overall electrode is compared in the aspect of specific capacity and volumetric capacity. Fabric electrode shows superior properties in specific capacity. It originates from carbon fabric (current collector) which is reactive with lithium ion, and coincides with our original objectives. However, the volumetric capacity of fabric electrode is smaller than that of fabric electrode. It could be overcome by adjusting the porosity of carbon fabric. According to JNTG Company, the porosity of used carbon fabric is almost 90 %. Thus, it is possible to increase the volumetric capacity by decreasing the extent of porosity.

**Table 2.** The comparison of specific capacity and volumetric capacity for two electrodes

| | $Cu_6Sn_5$-deposited carbon fabric electrode | $Cu_6Sn_5$-coated Cu foil electrode |
|---|---|---|
| Specific capacity of electrode* / mA h $g^{-1}$ | 288 | 168 |
| Specific capacity of current collector** / mA h $g^{-1}$ | 200 | 0 |
| Wt. ratio of $Cu_6Sn_5$ to current collector*** | 1 : 1.1 | 1 : 1.1 |
| Wt. ratio of $Cu_6Sn_5$ to conductive carbon/binder | 1 : 0 | 5.67 : 1 |
| Specific capacity of $Cu_6Sn_5$ / mA h $g^{-1}$ | 383 | 381 |
| Volumetric capacity of electrode**** / mA h $cm^{-3}$ | 113 | 178 |

*From the de-lithiation capacity in the first cycle in Figure 10a and 10b, in which the specific capacity is calculated on the basis of the total electrode mass.

**From the de-lithiation capacity in the first cycle in Figure 10c, in which the specific capacity is calculated on the basis of the mass of carbon fabric.

***The weight ratio was fixed at the same value for two electrodes.

****The electrode thickness was measured in the fully lithiated state for two electrodes.

**Table 3.** The comparison of thickness and weight for two electrodes

| | **Before deposition/coating** | **After deposition/coating** |
|---|---|---|
| Thickness of carbon fabric | 242 micron meters | 242 micron meters (SOC 0) / 271 micron meters (SOC 100) |
| Thickness of Cu foil | 4 micron meters | 24 micron meter (SOC 0) / 59 micron meter (SOC 100) |
| Weight of carbon fabric | 5.57 mg $cm^{-2}$ | 10.69 mg $cm^{-2}$ |
| Weight of Cu foil | 3.00 mg $cm^{-2}$ | 6.23 mg $cm^{-2}$ |

The safety of battery has relation with thickness change of electrode during cycling. As electrode experiences severe thickness increase during cycling, it might be swelled up and the package of battery could be damaged. It can lead to the leakage of electrolyte from battery. In this situation, free spaces in fabric electrode can be used to relieve the risk occurred by volume expansion of active material. Figure 12 indicates ex-situ measurement in thickness change of fabric electrode and conventional electrode. It is shown that the extent of thickness change is about 10 % at the fully lithiated state in fabric electrode (Figure 12a). On the other hands, the extent of thickness change is about 170 % at fully lithiated in conventional electrode (Figure 12b). The kind of active material used in both electrode is same, and the volume expansion experienced by active material is equal. Nevertheless, the structural difference in electrodes makes contrast on ability related with accommodating the volume change of active material at the inner part of electrode, which is reflected in thickness change. Consequentially, the safety of battery can be improved by using fabric electrode. Also, the volume expansion/contraction in restricted space frequently leads to crack formation in the active material particles, pulverization, particle detachment from the electrodes, and heavy deposition of resistive surface films on electrodes, all of which can lead to cell failure.

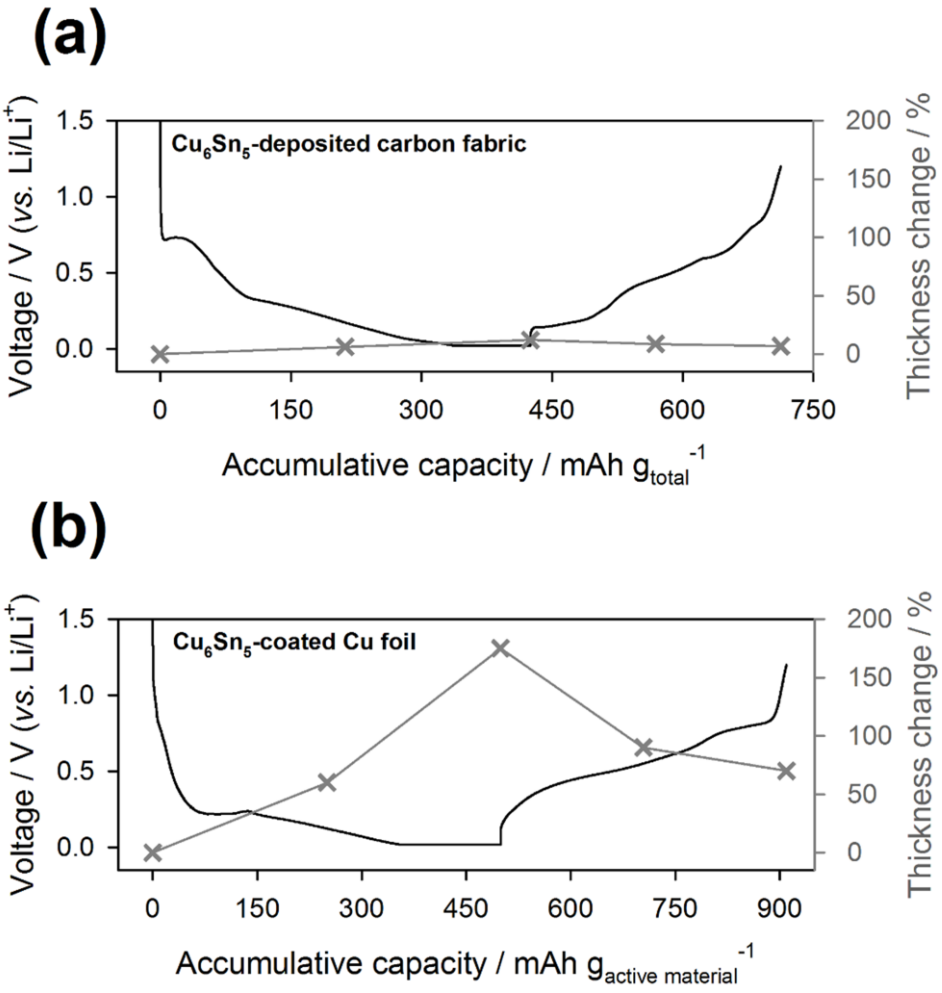


**Figure 12.** The lithiation/de-lithiation voltage profiles (black) and the variation of electrode thickness (grey).

Because there is no use in binder, volume change experienced by active material during cycling can easily lead to detachment of active material from carbon fabric. Therefore, the ex-situ FE-SEM image of $Cu_6Sn_5$-deposited fabric electrode is investigated at 10th delithiated states. When using $Cu_6Sn_5$ as shell material, there is no detachment of active material from carbon fabric (Figure 13a). It is well known that Cu acts a role as buffer matrix, and relieve the volume change during cycling. In addition, large cavities among carbon fibers gives active material sufficient space to expand during lithiation. As a results, it leads to good performance in cycleability (Figure 10d). Instead, the morphology of $Cu_6Sn_5$ transformed greatly compared with pristine (Figure 7e). The particle size of active material gets smaller, and the boundary of particles becomes clear.

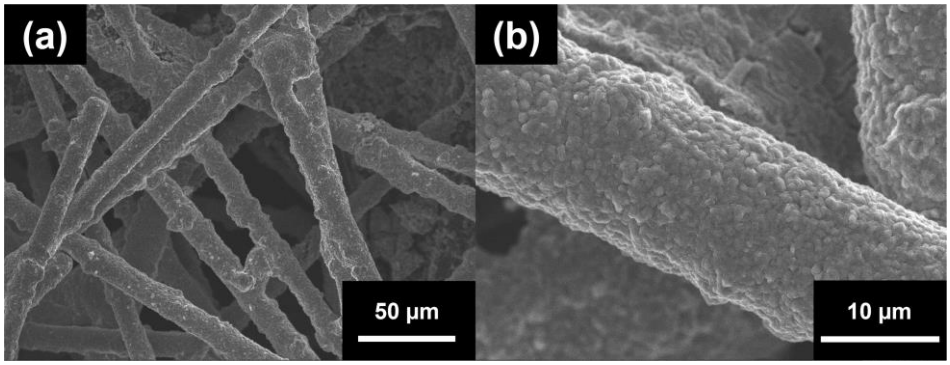


**Figure 13.** (a); FE-SEM image taken from the $Cu_6Sn_5$-deposited carbon fabric electrode after the $10^{th}$ de-lithiation. (b); the magnified view of (a).

### 3.1.4. Graphite embedding into carbon fabric to generalize its use as a current collector

By using the carbon fabric as a current collector, it is possible to develop the distinct negative electrode, materially and structurally. The specific capacity of negative electrode, which adopts the carbon fabric as a current collector, is increased by utilizing the materially distinct feature of the carbon fabric, which reacts with lithium-ion during electrochemical cycling. The structurally distinguishable characteristic of the carbon fabric is about uniform distribution of current collector over the whole electrode. The electrode is composed of electrode layer and current collector, and the electrode layer is made up by active material, binder and conducting agent. Usually, a current collector is separated with an electrode layer. When the thickness of electrode layer is about 50 μm, the active material located in top-most of the electrode layer is apart from current collector at the distance of 50 μm. However, in the case of carbon fabric, which locates uniformly over the whole electrode, the distance between active material and current collector can be decreased drastically. Thus, the current collector can easily collect the electronic flow over the whole electrode, and it is expected that the electrode composed of carbon fabric shows the better power capability than the conventional electrode, which uses Cu foil as a current collector. In this experiment, the novel electrode constitution and its preparation method are suggested to make the best use of carbon fabric current collector.

To realize the mentioned concept of fabric electrode, which uses a carbon fabric as a current collector, the simple method for active material preparation must be invented. To this end, the fabric electrode was soaked with the prepared slurry, whose viscosity was extremely decreased to penetrate into the carbon fabric current collector. The slurry was composed of active material, binder, conducting agent and the excess amount of N-Methyl-2-Pyrrolidone (NMP). Graphite, which is known to experience less volume change during electrochemical cycling, was used as

an active material, and the weight ratio of active material, binder and conducting agent was 90:5:5. After the soaking process of the slurry into the carbon fabric current collector, the void space is filled with the active material. Thus, the prepared electrode is expected to deliver not only the large specific capacity, which is a distinct property by using lithium-reactive current collector, but also the enormous volumetric capacity, which is an additional feature by this novel concept.

The manners for graphite embedding are categorized into bar-type method and map-type method (Figure 14). In bar-type method, a piece of carbon fabric was placed onto suction equipment, and the prepared slurry was put onto the carbon fabric along edge side. After mounting, the slurry was spread evenly upon the carbon fabric by doctor blade. In this process, suction was simultaneously conducted for 3 mins to make slurry penetrate into the carbon fabric. In map-type method, a piece of carbon fabric was placed onto suction equipment, and the prepared slurry was put onto the carbon fabric evenly. After mounting, the same process with bar-type method was conducted. The penetration degree of slurry during suction was checked by parchment paper placed between carbon paper and suction equipment. As the slurry is penetrated into carbon paper, the parchment paper would be wet with the slurry, and as it is not, the parchment paper would not be wet (Figure 15).

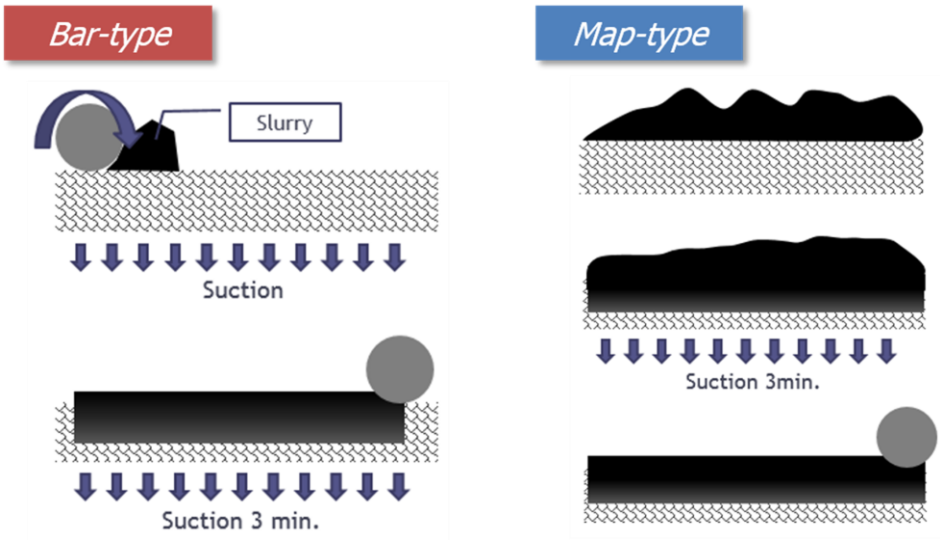


**Figure 14.** Two methods for embedding additional material into the carbon fabric by suction equipment.

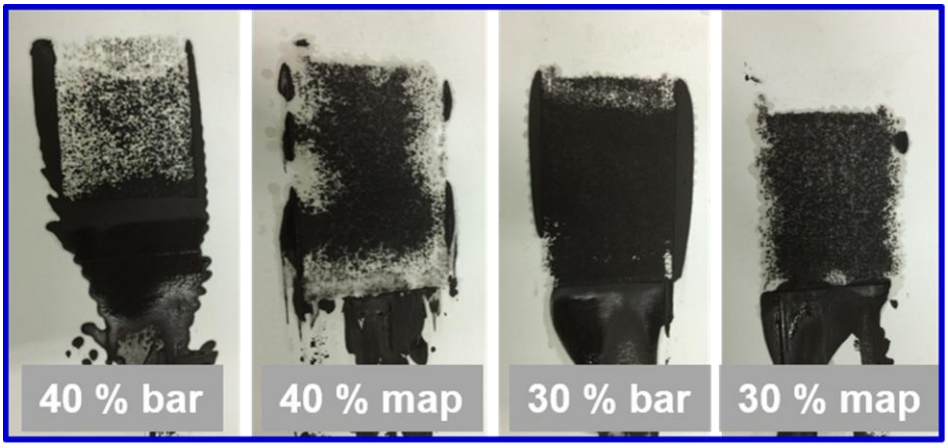


**Figure 15.** Penetration degree check by observing parchment paper placed between the carbon fabric and suction equipment.

Three kinds of slurry was prepared, depending on the weight ratio of solid content (active material, binder and conducting agent). The kinds of weight ratio are 50 %, 40 % and 30 %. It is expected that as the weight ratio of solid content is decreased, it is easy for the prepared slurry to penetrate into the carbon fabric. In fact, when the parchment paper was checked how it was wet with the slurry after suction process, the prepared slurry, which was composed of the 30 *wt.* % of solid content, showed the most superior ability related with penetration degree. The information about weight and thickness of the electrodes after suction process is summarized as Table 4 and Table 5. Reference in the table means the carbon fabric before suction process. When the information about weight is closely inspected, the contents of loaded slurry onto carbon fabric is larger in 50 % than in the others. Also, the contents of loaded slurry onto carbon fabric is larger in map-type than bar-type. However, it is another matter that the loaded slurry was successfully soaked into the carbon fabric. It can be illuminated by information about the thickness of the electrodes. According to table, when the solid content of the prepared slurry was smaller, the thickness of the electrodes after suction process was more similar with that of reference. In other words, when the slurry composed of 50 *wt.* % solid content was used to load active material into the carbon fabric, a large amount of the slurry remained upon the carbon fabric, and it made the thickness of composite electrode be larger than that of reference. Otherwise, when the slurry composed of 30 *wt.* % solid content was used, most of the slurry penetrated into the carbon fabric, and the thickness of composite electrode was similar with that of reference. Also, bar-type method is more desirable than map-type method in the aspect of penetration degree. Thus, bar-type method using the slurry of 30 *wt.* % was applied to load the active material into the carbon fabric, and the prepared electrode was used to examine the various properties.

**Table 4.** The weight information of embedded electrode.

| Weight (mg) | 50 % | 40 % | 30 % |
|---|---|---|---|
| Reference | 10.4 | 8.8 | 8.8 |
| Bar | 36.5 | 29.8 | 24.7 |
| Map | 55.6 | 45.1 | 42.2 |

**Table 5.** The thickness information of embedded electrode

| Thickness (um) | 50 % | 40 % | 30 % |
|---|---|---|---|
| Reference | 230~250 | 260~270 | 260~270 |
| Bar | 330 | 325~330 | 300 |
| Map | 430 | 380 | 390 |

The morphology of prepared electrodes are confirmed by FE-SEM experiments (Figure 16). The void spaces among carbon fibers are well shown in the reference electrode. After suction process, carbon fibers are not shown any longer in the top-most image, because of the graphite powder used as an active material of the slurry. In the cross-sectional image of composite electrode, it is checked that the slurry was penetrated into the carbon fabric uniformly. When closely inspecting the information about weight and thickness, the weight of slurry loaded was about 1.8 times of the carbon fabric, and most of the slurry was penetrated into the carbon fabric.

Voltage profiles of carbon fabric electrode and graphite embedded carbon fabric electrode are shown in Figure 17. The capacity delivered above 0.3 V (*vs.* $Li/Li^+$) comes from non-graphitized carbon of carbon fabric current collector. The capacity share above 0.3 V (*vs.* $Li/Li^+$) is shortened in graphite embedded carbon fabric electrode, because of active material loaded into carbon fabric. Also, the specific capacity of embedded electrode is increased, compared with that of carbon fabric electrode. The ideal reversible capacity of graphite is 372 mA h $g^{-1}$, and the reversible capacity of carbon fabric is about 200 mA h $g^{-1}$. Thus, when the weight ratio of active material is increased, the specific capacity, calculated from the weight of whole electrode, must be increased. The capacity information of carbon fabric electrode and embedded electrode is summarized as table 6. All kinds of capacity are increased in embedded electrode, and especially, the volumetric capacity of embedded electrode is 1.3 times larger than that of carbon fabric electrode. In the case of fabric electrode, volumetric capacity is a weak point, and it arises from uniformly distributed void spaces among carbon fibers. When graphite is embedded into carbon fabric, the empty spaces are filled with an active material, and it increases the volumetric capacity. It is concluded that the simple method for loading active material into carbon fabric is invented to generalize its use as a current collector and the weak point related with volumetric capacity is overcome by mounting additional active material in empty spaces of carbon fabric current collector.

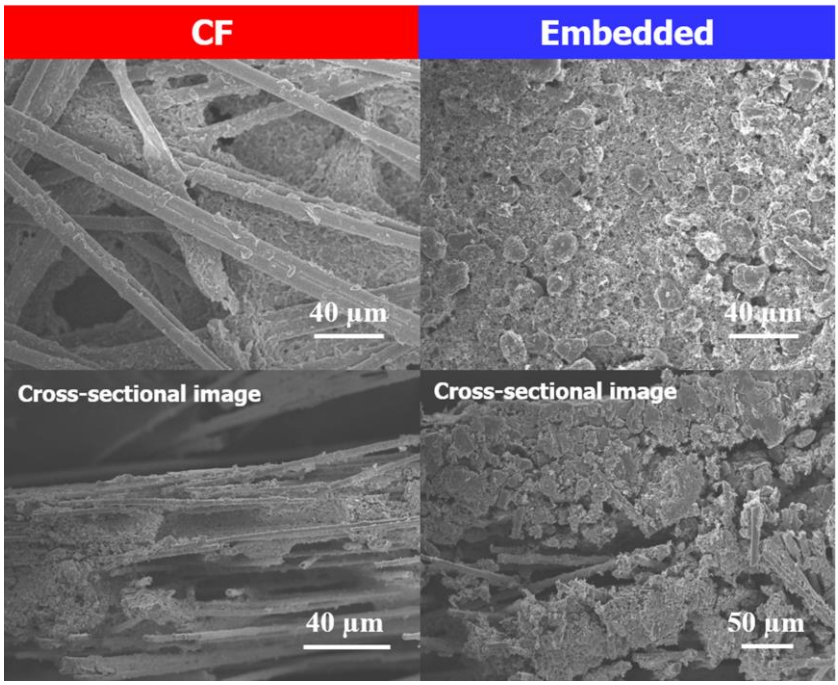


**Figure 16.** FE-SEM images of carbon fabric and embedded carbon fabric. The images are made from top-most and cross-section.

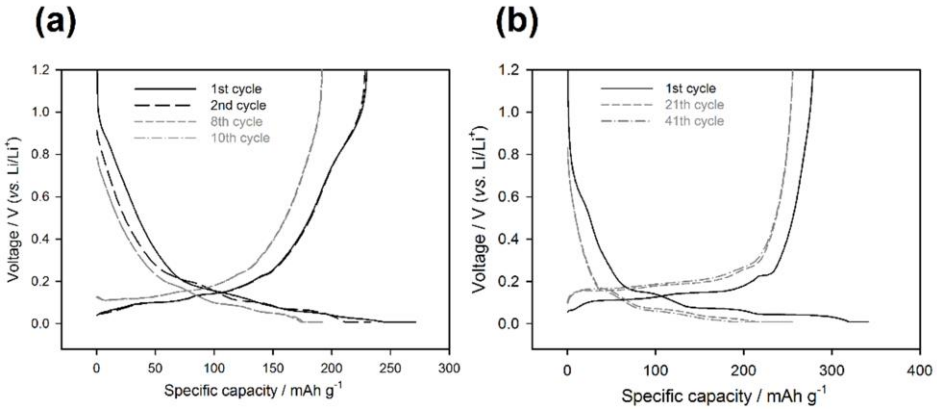


**Figure 17.** Voltage profiles of (a) carbon fabric electrode and (b) graphite embedded carbon fabric electrode.

**Table 6.** The information of carbon fabric and graphite embedded carbon fabric.

| | CF | Embedded CF |
|---|---|---|
| Specific capacity | 197 mA h $g^{-1}$ | 248 mA h $g^{-1}$ |
| Areal capacity | 1.04 mA h $cm^{-2}$ | 2.35 mA h $cm^{-2}$ |
| Volumetric capacity | 38 mA h $cm^{-3}$ | 86 mA h $cm^{-3}$ |

### 3.1.5. Summary of section

In this research, $Cu_6Sn_5$-deposited fabric electrode which has the unique structure of carbon fiber (core) – $Cu_6Sn_5$ alloy (shell) is successfully prepared and utilized as a negative electrode. Carbon fabric plays the role of not only current collector but active material. In conventional electrode, Cu foil used as a current collector has no reactivity with lithium ion. Thus, when the weight of overall electrode including current collector is considered, the specific capacity of electrode decreases dramatically. In the case of composite fabric electrode, current collector which is made up of carbon fiber shows the reactivity with lithium ion. Thus, the specific capacity of electrode could be higher than that of conventional electrode.

The reactivity of graphite in carbon core – $Cu_6Sn_5$ shell fabric electrode is confirmed. The XRD peak of $LiC_6$ is well shown, and the overpotential experienced by graphite is rather smaller in composite fabric electrode than carbon fabric electrode. It is estimated that the difference comes from electric conductivity of electrode. The insufficient electric conductivity of carbon fabric is supplemented by shell material which is known to be highly conductive. Also, it is calculated that the reactivity of shell material is maintained compared with active material on conventional current collector.

There are several advantages in use of fabric electrode which has the porous structure. There is a big difference in the presence of sufficient cavity between fabric electrode and conventional electrode. Cavity relives the volume change of active material during cycling. When there is no sufficient space to accommodate volume expansion, it is inevitable to increase in the thickness of electrode during lithiation. This phenomenon has a bad effect on the package of battery, and it makes the configuration of battery unstable. In this aspects, fabric electrode has the sufficient space, and it results in the improvement of battery safety. Also, massive volume change of active material usually leads to crack generation, pulverization, additional electrolyte decomposition,

detachment of material and capacity fading. In fabric electrode, these volume change can be effectively controlled, thus the electrode performs reasonably good cycle retention.

The general methods for active material loading into carbon fabric is invented to expand the utility of carbon fabric as a current collector. It is possible to load active material into carbon fabric by slurry suction process, which is simple. The methods are categorized into bar-type and map-type. As a result, penetration degree of active material is high by bar-type method. Also, the solid content ratio of slurry is researched as a variable, and 30 % solid content shows a most desirable property as a slurry. It is confirmed by FE-SEM images that the penetration of active material into carbon fabric was well done. Also, it is realized that the active material participates in delivering capacity in the composite electrode.

## 3.2. High performance negative electrode by using flexible and conductive stainless steel fabric as a current collector

### 3.2.1. Strategies for flexible and high rate capable negative electrode

At present, lithium-ion batteries (LIBs) are considered as one of the most promising energy storage systems because of their superior performances such as high capacity, stable cycle performance and high power capability [59, 62, 64]. In real, LIBs are now expanding their market from small mobile devices to electric vehicles. However, when it comes to the field of wearable electronics, in which the flexibility of their components becomes more important, the

design of conventional LIBs should be changed. As such, this paper describes our efforts to construct an LIB that could survive the daily strain of being used in wearable electronic devices. To this end, many factors need to be considered [72, 73].

The conventional LIBs use metal foils as the current collector, onto which active materials are coated together along with conductive carbons and polymeric binders. When the conventional electrodes are bended or folded, the active materials are frequently detached from the current collector (Figure 18). One reason for this must be the uneven stress dissipation; stress is dissipated over the 2-dimensional plane, but poorly along the other direction (for example, the vertical direction of metal foil). To solve or at least mitigate this problem, metal foils are modified or other types of current collector have been tried [74-76]. Among those, a 3-dimensional carbon-based current collector was found to effectively dissipate mechanical stress, obviously due to its 3-dimensional structure [14, 75, 77, 78]. In this work, stainless steel (SUS) fabric that has a 3-dimensional network structure is tested as a current collector. Here, an expectation was that it not only provides a 3-dimensional electrically conductive network as a current collector but effectively dissipates the stress upon bending or folding.

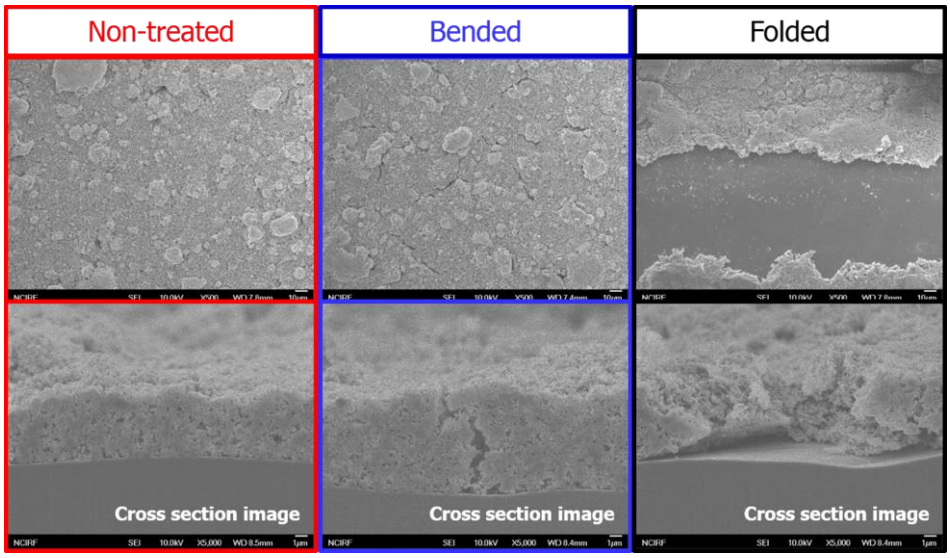


**Figure 18.** FE-SEM images of the conventional electrode before and after several flexibility test (bending and folding).

In order to take advantage of SUS fabric as a current collector for flexible batteries, the active electrode materials and their deposition methods should be carefully considered. Here, the adhesion strength at the interface between active material and current collector, among others, seems to be critical because the detachment of active material from current collector is most frequently observed upon bending or folding. In this work, the liquid-phase deposition method, which gives a strong adhesion between deposit and substrate via covalent bond formation, was utilized to deposit active material onto the SUS fabric [79]. Furthermore, the liquid-phase deposition is effective to coat oxide materials onto complex substrates such as SUS fabric being used in this work [80, 81]. Namely, the conventional slurry coating cannot be employed to coat active materials on the SUS fabric because the slurry pasting is not uniform; the deposition is easier onto the outmost surface of SUS fabric but it is difficult to squeeze the slurry into the void spaces that are highly populated inside the 3-dimensional network structure. In contrast, the liquid-phase deposition is effective for uniform deposition on SUS fabric because the precursor solution can easily penetrate into the void spaces [80, 81]. Usually, there are two factors making the application of liquid-phase deposition be difficult in preparing electrode materials. Firstly, the loading of active electrode material is limited. In particular, if the electrode material has low electronic conductivity (for example, $TiO_2$), the electrode layer should be thin. In this work, we use the stainless steel (SUS) fabric as a current collector, onto which $TiO_2$ layer is deposited by liquid-phase deposition. Note that the SUS fabric has high surface area. Although the thickness of $TiO_2$ layer on the SUS fabric is thin (about 1.5 μm), the $TiO_2$ loading on the SUS fabric is much larger compared with the conventionally used metal foil. This is one of the novel ideas. Secondly, the selection of current collector is limited. In general, heat-treatment is required in liquid-phase deposition to remove the fluorine-containing impurities that are generated during the deposition. Normally, the heating temperature is as high as 500 $^{o}$C, which is high enough to oxidize the current collector (such as Cu foil). Fortunately, the SUS fabric is stable against

oxidation at this temperature. In short, the use of SUS fabric can overcome the problems involved in the liquid-phase deposition method.

The next task is the selection of active materials. Some of the negative electrode materials suffer from a massive volume expansion/contraction upon electrochemical cycling, such that the active materials themselves are prone to being cracked or pulverized due to mechanical strain. The electrode detachment is severe and will be more serious when used for flexible batteries due to the additional massive mechanical stress caused by folding or bending. Considering this feature, the zero-strain materials, which are free from severe volume change, are the right selection for the flexible batteries. In this work, as the zero-strain material, $TiO_2$ was selected [82]. The liquid-phase deposition of $TiO_2$ was successfully carried out on mesoporous carbon in the previous work. Hence, we prepared the $TiO_2$–deposited SUS fabric by taking the reported procedure.

The primary objective of this work was to realize a flexible electrode by combining the SUS fabric, $TiO_2$ electrode and liquid-phase deposition method. The uniform deposition of $TiO_2$ particles onto the SUS wires located inside the fabric was confirmed. The adhesion strength was assessed by using a peel test. To examine the flexibility of the prepared electrodes, the folding test was performed, in which a massive stress was imposed on the $TiO_2$-deposited SUS electrodes, and any changes in the electrode integration and electrode performances were examined.

### 3.2.2. Characterization of deposited SUS fabric

The growth mechanism of $TiO_2$ on SUS substrate by liquid-phase deposition is illustrated in Figure 19 [79, 83]. Hydrogen of surface hydroxyl group at SUS substrate is associated with fluorine of titanium precursor, and it leaves as the form of HF. As a result, iron of SUS fabric is connected with titanium of deposit by bridging oxygen, and it means that deposit is strongly

attached to substrate by covalent bond. $TiO_2$ layer continuously grow in the same way. The equation of chemical reaction during deposition is summarized as follows [79, 83]:

$$[TiF_6]^{2-} + 6H_2O \rightleftharpoons [Ti(OH)_6]^{2-} + 6HF \quad (1)$$

$$[Ti(OH)_6]^{2-} + 2H^+ \rightarrow TiO_2 + 4H_2O \quad (2)$$

$$H_3BO_3 + 4HF \rightarrow HBF_4 + 3H_2O \quad (3)$$

When HF is generated during hydroxylation of titanium precursor ($TiF_6$), it is removed by the excess amount of boric acid (Equation 3). Thus, the equilibrium of the first reaction inclines to the direction of hydroxylation, and the following reaction, growth of $TiO_2$ layer, continues (Equation 1). Usually, the deposit is attached to substrate strongly by covalent bond, which makes the prepared electrode resistive to the external stress occurred during flexible test. Also, the deposit prepared by liquid-phase deposition covers the substrate uniformly, and it is attributed to the dissolved state of precursor during deposition and slow kinetics for deposition ruling the problem engaged with mass transfer out. However, there exist some impurities such as fluorine, and the impurities could hinder the reactivity of deposit with lithium ion. Thus, heat-treatment in air condition is conducted to substitute the fluorine with oxygen [83].

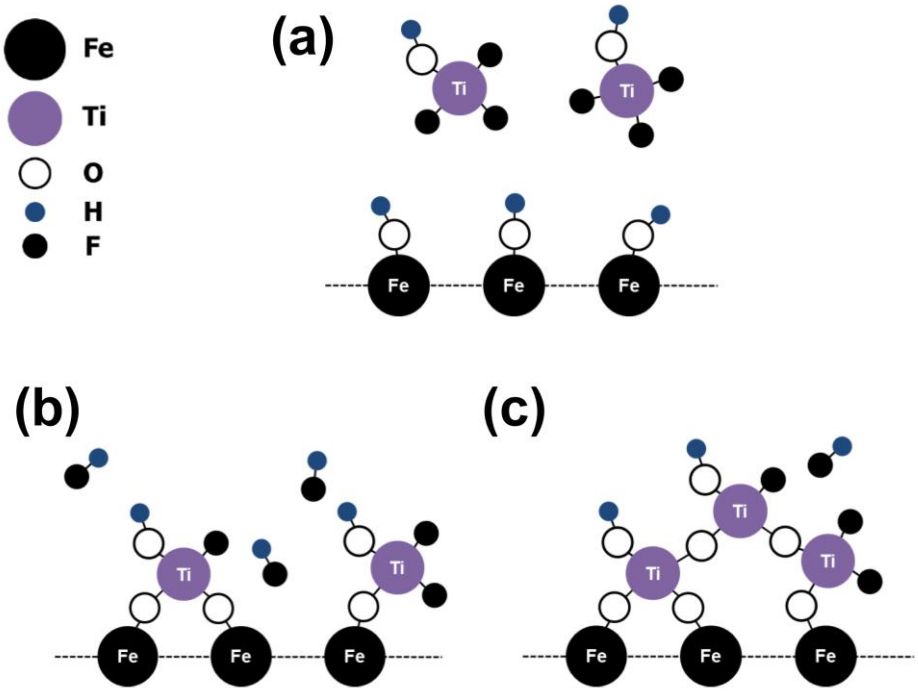


**Figure 19.** Growth mechanism of $TiO_2$ on SUS substrate by liquid-phase deposition.

There are FE-SEM images of SUS fabric in Figure 20a-c. As seen in Figure 20a, SUS fiber constructs the 3-dimensional network to form non-woven fabric, and the diameter of the fiber is about 7 μm (Figure 20b). When SUS is utilized as a current collector, the 3-dimensional structure dissipates the imposed stress effectively during flexible test [76], such as bending and folding, and the problem occurred by imposed stress, like detachment of active material, could be relieved. Carbon-based 3-dimensional structured current collector have been researched for flexible electrode by the virtue of its stress-dissipation property. SUS fabric resembles the property of structure, but differs in its superior electric conductivity than that of carbon-based one. The basic role of the current collector is to facilitate the electron flow between active material and external circuit. Thus, SUS fabric is more desirable as a current collector than carbon-based one. As shown in the cross-sectional image of SUS fiber (Figure 20c), there is no phase boundary and the phase is homogeneous. There are FE-SEM images of deposited SUS fabric in Figure 20d-f. The overall structure is consistent with SUS fabric, and the deposition is conducted uniformly (Figure 20d). Deposit-layer is composed of nano-sized spherical particles (Figure 20e), and the thickness of deposit-layer is about 1.5 μm (Figure 20f). Cracks are found on the deposit layer (Figure 20e), which must be generated during the drying process due to shrinkage caused by water evaporation. Active material is deposited onto SUS fabric by liquid-phase deposition in the microstructure of core (SUS fiber)/shell (active material), and the deposition is carried out evenly in radial direction.

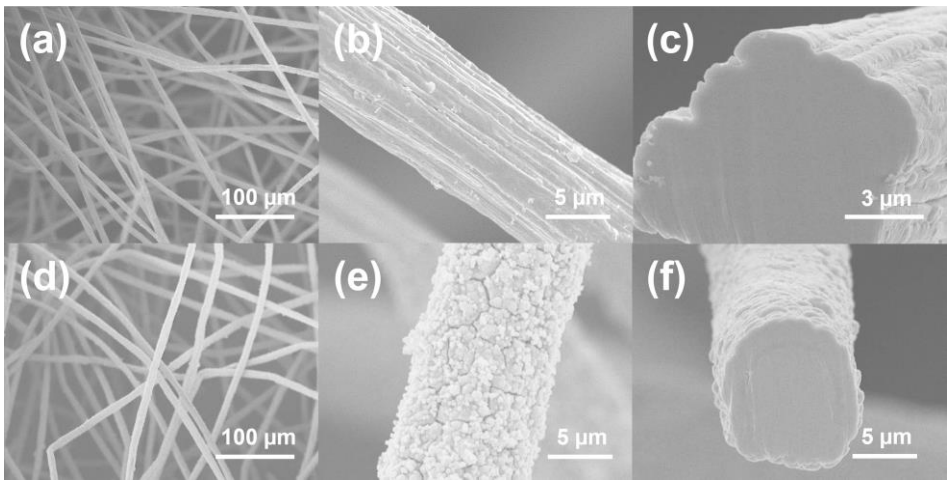


**Figure 20.** FE-SEM images of (a), (b), and (c) SUS fabric and (d), (e), and (f) $TiO_2$-deposited SUS fabric. Cross-sectional images of (c) SUS fabric and (f) $TiO_2$-deposited SUS fabric.

The analysis on phase and morphology of deposit is conducted by XRD and TEM experiment, and, to this end, precipitated powders are collected after the process of liquid-phase deposition (Figure 21a,b). The collected powder is calcined at 500 $^{o}$C in air condition during 5 h. As seen in XRD pattern (Figure 21a), the peaks of precipitated powder are exactly identical to that of anatase-TiO2, thus, the phase of deposit is confirmed as anatase-TiO2. As shown in TEM images (Figure 21b), precipitated particle is composed of primary particles of which the size is about 40 nm, and the overall size of secondary particle is roughly 250 nm. The shape of primary and secondary particle is both spherical. In the case of Raman experiment, SUS fabric, deposited SUS fabric and precipitated $TiO_2$ powder are analyzed (Figure 21c). All samples are heat-treated. As the intensity of peaks is much weak in fabric samples, the intensity of precipitated sample is weakened about 200 times, and all the graph are drawn together. The reason for weak intensity is related with void spaces and the surface non-flatness of fabric. The characteristic peaks of anatase-$TiO_2$ are shown in precipitated powder, and these peaks are well-matched with that of deposited SUS fabric at 395, 516 and 640 $cm^{-1}$. Thus, it could be inferred that the phase of deposit is anatase-$TiO_2$ [84]. The effect of heat-treatment in the process of liquid-phase deposition is confirmed by XPS experiment (Figure 21d). Strong fluorine peak can be observed in the non-treated $TiO_2$-deposited SUS fabric, which confirms the presence of fluorine impurities. As expressed in reaction mechanism of liquid-phase deposition, it is hard to substitute the fluorine with oxygen completely by using excess boric acid. When there is F-impurities, the phase of deposited material is not a perfect anatase-$TiO_2$, and the reactivity with lithium-ion is hindered. Thus, removal of F-impurities is important, and the perfect replacement of fluorine with oxygen could be achieved by heat-treatment. After heat-treatment, there is no peaks in F1s spectra, and it can be confirmed that $TiO_2$-deposited SUS fabric is successfully prepared with no impurities.

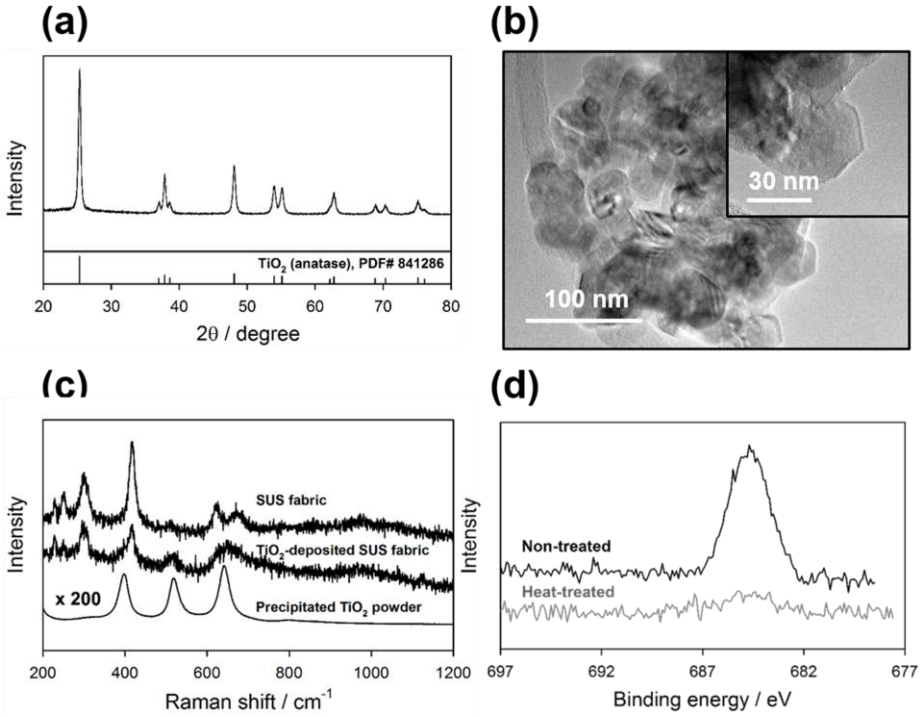


**Figure 21.** (a); XRD pattern for precipitated powder during LPD process. (b); TEM images for precipitated $TiO_2$ powder. The magnified TEM image of a primary particle is presented in the inset of (b). (c); Raman spectra of SUS fabric, $TiO_2$-deposited SUS fabric, and precipitated $TiO_2$ powder. (d); XPS F1s spectra of $TiO_2$-deposited SUS fabric before and after heat-treatment.

In this research, voltage cut-off range during electrochemical cycling was from 1.5 V (*vs.* $Li/Li^+$) to 2.5 V (*vs.* $Li/Li^+$). The reason for cut-off selection comes from regulation of electrolyte decomposition. In this condition, if the $TiO_2$ is not sufficiently crystallized, the shape of voltage profile will be sloped, and the $TiO_2$ cannot deliver the capacity itself, because of the voltage cut-off. Fortunately, the degree of crystallization is sufficiently grown during heat-treatment process, and it is confirmed by various experimental tools. Firstly, it is checked by XRD data (Figure 22a). The characteristic peaks of anatase-$TiO_2$ is well shown in the two samples (before and after heat-treatment). Especially, the main peak at 25 $^o$ becomes sharp after heat-treatment process. Thus, it can be concluded that $TiO_2$ becomes crystallized by heat-treatment. Also, this conclusion can be reinforced by extended X-ray absorption fine structure (EXAFS) result (Figure 22b). The kind of peaks is almost same in the two samples (before and after heat-treatment). Also, the peak intensity of short range order, which is seen below 2 Å, is similar between the two samples. However, beyond 2 Å, the peak intensity of the heat-treated sample is stronger than that of the non-treated sample. Thus, it is confirmed again that the degree of crystallization is increased by heat-treatment.

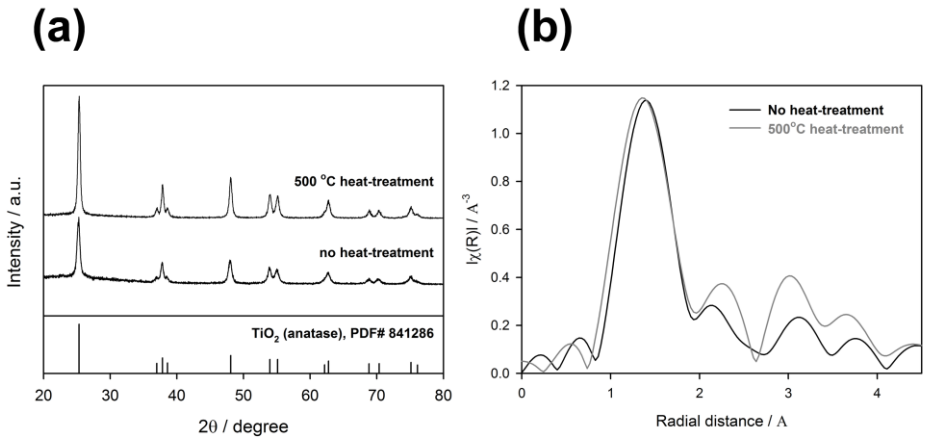


**Figure 22.** (a); XRD data and (b); extended X-ray absorption find structure (EXAFS) results of precipitated powder before and after heat-treatment.

### 3.2.3. Confirmation of the adhesion strength retained by liquid-phase deposition

Adhesion strength between active material and current collector is important to prepare flexible electrode which is resistive to external stress. Adhesion strength can be retained in the process of liquid-phase deposition. In detail, during liquid-phase deposition, active material grows upon the substrate with covalent bond, and this covalent bond assures the strong adhesion strength. Thus, if the presence of covalent bond is confirmed, it can be concluded that there is strong adhesion strength. However, the amount of covalent bond, which is formed through one-layer, is too scarce to be detected by spectroscope, such as Raman spectroscopy. Thus, we trace the evidence for covalent bond by another experiment.

Figure 23a shows O1s spectra by X-ray photoelectron spectroscopy of three substrates which was pre-treated differently from each other. In the case of 'Ar-treated' that was heat-treated at 300 $^{o}$C in Ar condition, surface hydroxyl group is effectively removed. 'Non-treated' presents higher density of hydroxyl group than 'Ar-treated', and 'Piranha-treated', which was pre-dipped in piranha solution in 80 $^{o}$C for 30 min, shows the highest density of hydroxyl group in three samples. The density of hydroxyl group can be confirmed from MOH peak. When the peak is strong, the density of group, represented by the peak, is high. Bulk oxygen peak is weak in 'Piranha-treated' which has high density of hydroxyl group.

Adhesion strength between $TiO_2$ layer by liquid-phase deposition and SUS foil was inspected by peel test. $TiO_2$ deposition condition of three samples was different from each other, and three samples were treated in various conditions before liquid-phase deposition. In other words, liquid-phase deposition was conducted in three samples which were different in the degree of hydroxylation from each other. According to the suggested deposition mechanism, the density of covalent bond depends on the density of surface hydroxylation of substrate. Thus, if the adhesion

strength depends on the degree of surface hydroxylation, it can be concluded that the covalent bond is formed during liquid-phase deposition. As seen in Figure 23b, adhesion strength increases in the order of 'Ar-treated', 'Non-treated' and 'Piranha-treated', and the order is same with the degree of surface hydroxylation. Therefore, it can be inferred that $TiO_2$ is linked with substrate, such as SUS foil and SUS fabric, by covalent bond during liquid-phase deposition.

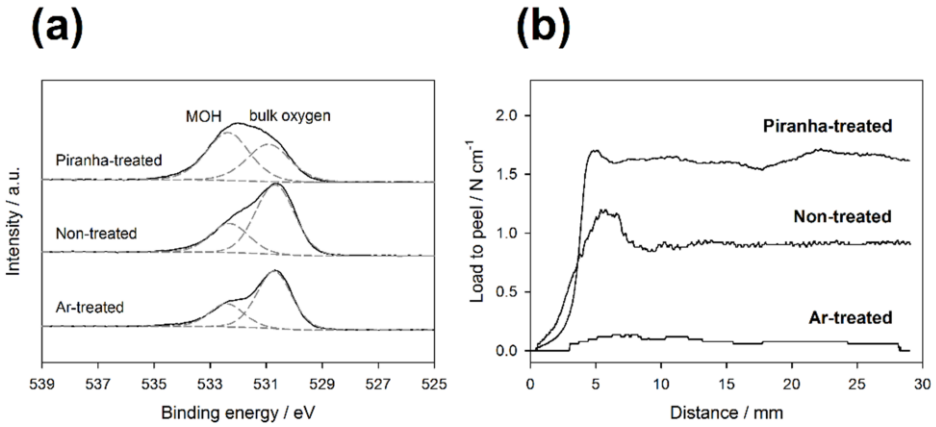


**Figure 23.** (a); XPS data of variously treated stainless steel (SUS) foil. (b); Peel test results of $TiO_2$-deposited SUS foils, which were pre-treated in the several conditions. All electrodes prepared were 10 mm wide and 60 mm long, and the speed of displacement was 30 mm $min^{-1}$.

In fact, it was checked by peel test how the adhesion strength by liquid-phase deposition is strong. And, the strength was compared with that of conventional binder system. In other words, the adhesion strength of $TiO_2$-deposited SUS foil by liquid-phase deposition is compared with that of $TiO_2$-coated Cu foil by conventional slurry coating. In the case of conventionally prepared electrode, PVdF binder was used to adhere the composite, in which active material and conducting agent are mixed, to Cu foil used as a current collector, and the amount of PVdF is about 5 *wt.* %. Considering that the $TiO_2$ layer deposited on the SUS foil was not detached by 3M adhesive tape (Figure 24b), the extent of adhesion strength between $TiO_2$ and SUS foil is above 5.551 N $cm^{-1}$ as shown in Figure 24a. In other words, the measured adhesion strength is related with interface between tape and $TiO_2$, and the adhesion strength of interface between $TiO_2$ and SUS foil is stronger than that between tape and $TiO_2$. In the case of composite electrode prepared with conventional slurry coating process, the extent of adhesion strength is 0.224 N $cm^{-1}$, which shows similar extent with reported one [85]. When active material is prepared by liquid-phase deposition, the extent of adhesion strength at the interface is at least 25 times larger than that of conventionally prepared one. Also, 5.551 N $cm^{-1}$ is higher than reported adhesion strength of polyurethane binder which is previously examined for flexible electrode [85]. This strong adhesion strength retained by liquid-phase deposition is essential for flexible electrode to endure the imposed stress during bending and folding.

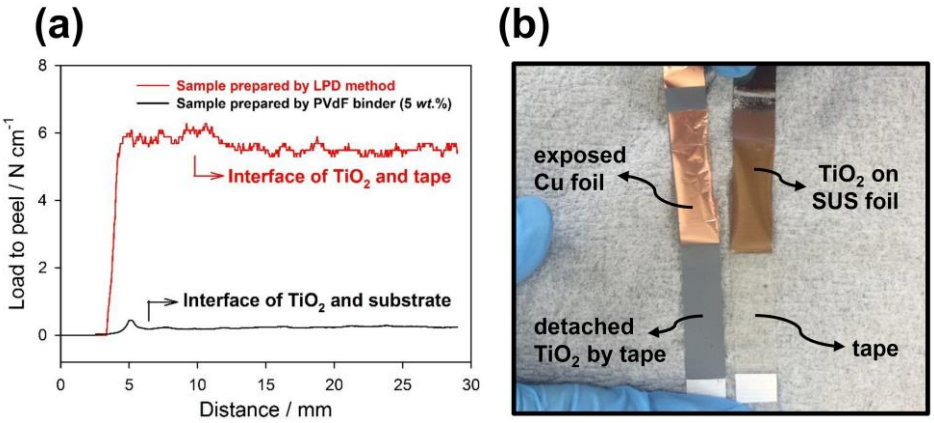


**Figure 24.** (a); Adhesion strength of $TiO_2$ electrodes to the substrate measured by peel test. (b); Side-by-side comparison of the peel tests performed on the two electrodes. All electrodes prepared were 10 mm wide and 60 mm long, and the speed of displacement was 30 mm $min^{-1}$.

### 3.2.4. The electrochemical test of $TiO_2$-deposited SUS fabric

Figure 25a shows the voltage profile of $TiO_2$-deposited SUS fabric electrode (coin-type cell). $TiO_2$-deposited SUS fabric shows its reaction plateau at 1.8 V (*vs.* $Li/Li^+$), and delivers the reversible capacity of 164 mA h $g^{-1}$ which is similar to the typical electrochemical properties of anatase-$TiO_2$ [86]. Figure 25b shows cycle performance of $TiO_2$-deposited SUS fabric electrode (coin-type cell). The cycle retention is very stable until 100th cycle, in which the capacity retention reaches about 98.8 %, and the Coulombic efficiency is always over 99 % except initial few cycles. Stable cycle retention is attributed to the property of $TiO_2$ experienced less volume change during electrochemical cycling [82]. In other words, initial adhesion strength retained by covalent bond is maintained even after electrochemical cycling, and it leads to stable cycle retention.

Also, maintenance of adhesion strength retained by liquid-phase deposition can be directly observed by *ex-situ* FE-SEM images (Figure 26). After $30^{th}$ delithiation, there are no detachment of active material, and the interface between $TiO_2$ and SUS fiber is well lasted. Even after $100^{th}$ delithiation, there are no detachment of active material, and thin SEI is confirmed by the accumulative electrolytic decomposition. Also, the interface between $TiO_2$ and SUS fiber is clear. Maintenance of adhesion strength is important for flexible electrode, because the stress during bending and folding is imposed at all time, even during electrochemical cycling. It can be inferred that the property of $TiO_2$ helps the electrode be flexible.

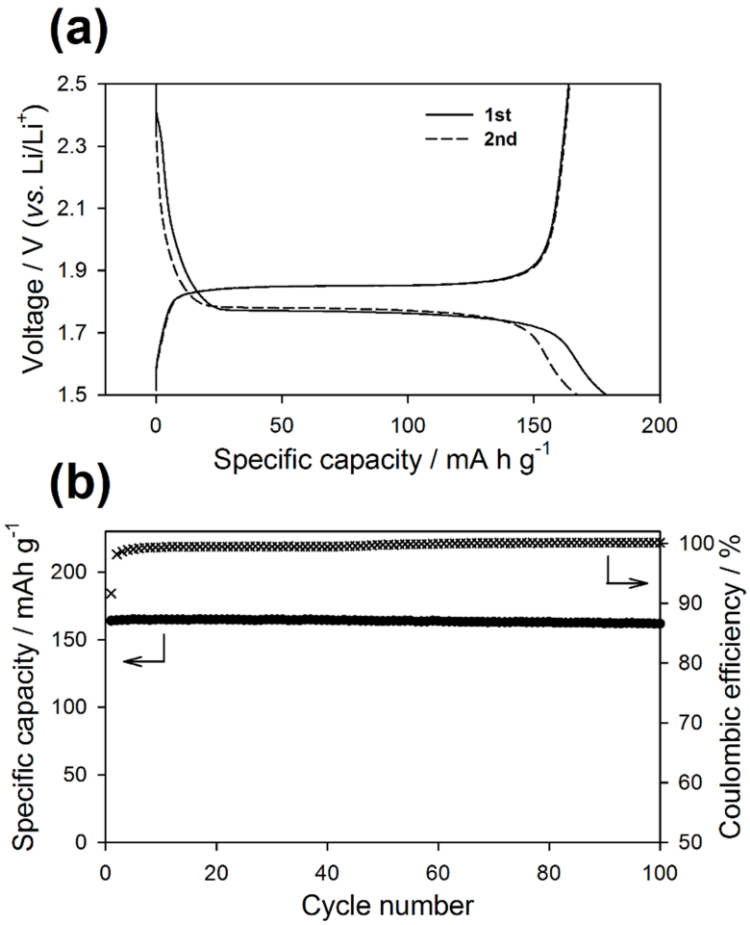


**Figure 25.** (a); Voltage profile of $TiO_2$-deposited SUS fabric electrode (coin-type cell). (b); Cycle performance. Electrochemical cycle number is plotted against specific capacity and Coulombic efficiency.

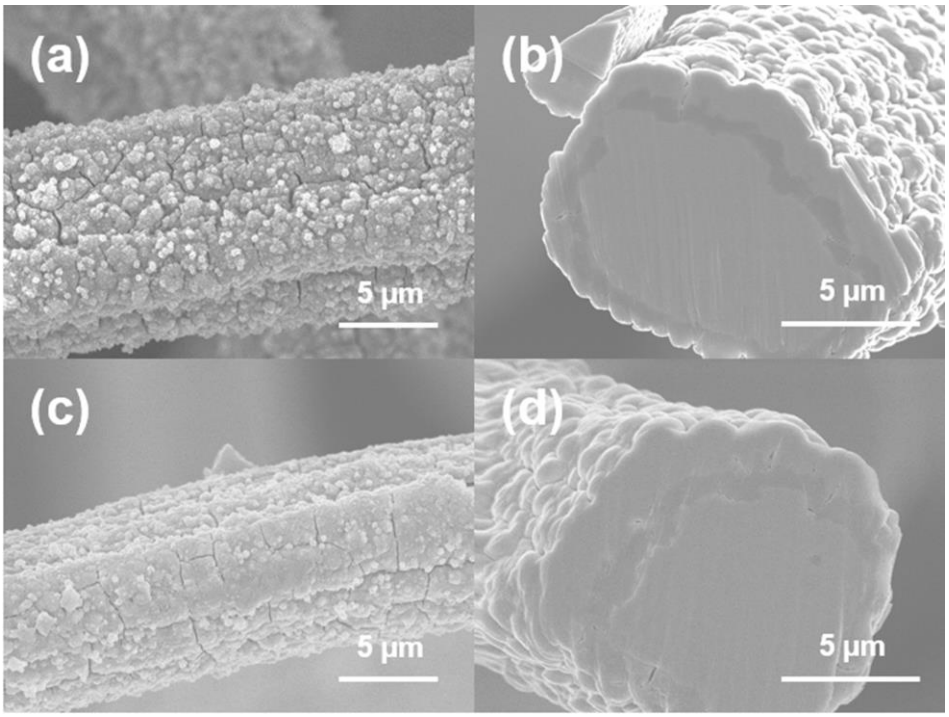


**Figure 26**. *ex-situ* FE-SEM images of $TiO_2$-deposited SUS fabric electrode after 30$^{th}$ delithiation (a), (b), and 100$^{th}$ delithiation (c), (d). (b), (d) are cross-sectional images of (a), (c), respectively.

### 3.2.5. The flexibility test of $TiO_2$-deposited SUS fabric

Optical images in Figure 27a-c show flexible properties of $TiO_2$-deposited SUS fabric such as bendable, rollable and twistable. During various flexible test, $TiO_2$-deposited SUS fabric is not undergone permanent deformation or detachment of active material from current collector. To maximize the imposed stress during flexible test, folding test was conducted (Figure 28). During folding test, bending radius is almost zero, and the utmost stress is imposed along the crease line. The folding and unfolding is repeated 30 times during folding test, and the state of crease line was observed by FE-SEM. In the case of $TiO_2$-deposited SUS fabric, there is no detachment of active material from current collector (Figure 28a). However, $TiO_2$-coated Cu foil prepared by conventional slurry spreading shows the detachment of active material from current collector, and the surface of Cu foil is exposed along the crease line (Figure 28b). The resistivity of $TiO_2$-deposited SUS fabric against stress generated during folding test comes from 3-dimensional structure of current collector and strong initial adhesion retained by liquid-phase deposition. The structure of SUS fabric alleviates the imposed stress effectively, and initial adhesion strength make a threshold of stress the active material could last higher. Even though $TiO_2$-deposited SUS fabric experiences electrochemical cycling and following folding test, there is no detachment of active material (Figure 28c), and the stable interface between active material and current collector is also maintained as seen in the cross-sectional image (Figure 28d). It is attributed to material characteristic of $TiO_2$ which undergoes less volume change during electrochemical cycling.

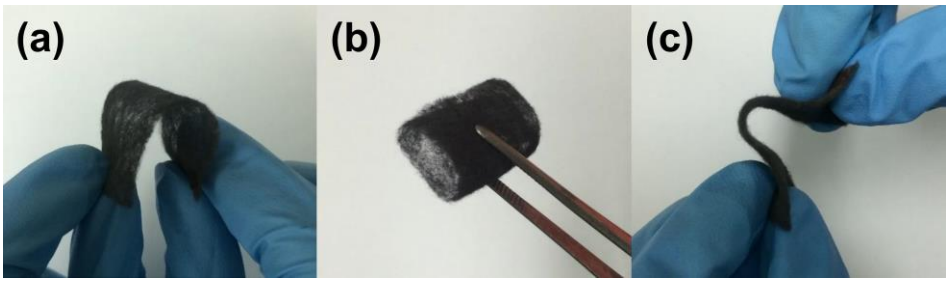


**Figure 27.** Optical images of $TiO_2$-deposited SUS fabric during bent (a), rolled (b), and twisted (c).

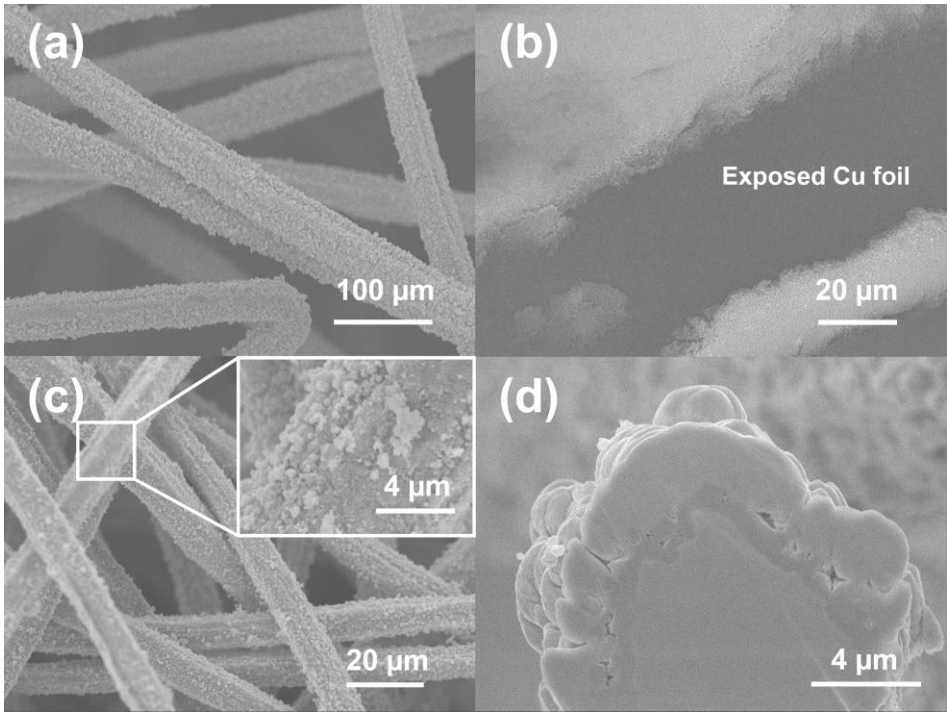


**Figure 28.** FE-SEM images of (a) $TiO_2$-deposited SUS fabric by LPD and (b) $TiO_2$-coated Cu foil by conventional slurry spreading after folding test. (c); FE-SEM images of $TiO_2$-deposited SUS fabric after 100 electrochemical cycles and subsequent folding test. (d); Cross-sectional image of (c).

To examine the effect of imposed stress on the electrochemical properties of $TiO_2$-deposited SUS fabric, the set of folding test is designed using Li/$TiO_2$-deposited SUS fabric pouch cell. It is possible, because, contrary to coin cell, pouch cell could be folded in the middle of electrochemical cycling [14, 77]. In the case of pouch cell, the folding test means the folding and unfolding the pouch cell 30 times, and the folding test is carried out every time at the end of each five electrochemical cycling. The electrochemical cycling of pouch cell was conducted for 25 times, and the accumulative times for folding and unfolding reached 120 times. As shown in Figure 29a, the set of folding test has no effect on voltage profile. Otherwise, decrease in specific capacity or change in polarization is presented in voltage profile by the imposed stress. Also, as seen in Figure 29b, the cycle retention is not affected by the folding stress. It means that the imposed stress is effectively dissipated and overcome by adopting the several points, such as SUS fabric, liquid-phase deposition and $TiO_2$.

Material selection of $TiO_2$ is based on the maintenance of adhesion strength. Also, when $TiO_2$ is used as an active material, it experiences less electrolytic decomposition, which precipitates to make SEI on the surface. SEI can be damaged by the imposed stress during flexible test, and it decreases the Coulombic efficiency to supplement the exposed surface by the newly generated SEI. According to the linear sweep voltammetry using Cu electrode, the amount of electrolytic decomposition is tiny above 1.5 V (*vs.* $Li/Li^+$) (Figure 30a). The quantity of electrolytic decomposition is only 8.6 % above 1.5 V (*vs.* $Li/Li^+$), and the major portion takes place under 1.5 V (*vs.* $Li/Li^+$) (Figure 30b). The operating potential range of $TiO_2$ is from 1.5 V (*vs.* $Li/Li^+$) to 2.5 V (*vs.* $Li/Li^+$). Thus, it can be inferred that SEI formation on the surface of $TiO_2$ is less, and the instability of Coulombic efficiency during the flexible test can be minimized.

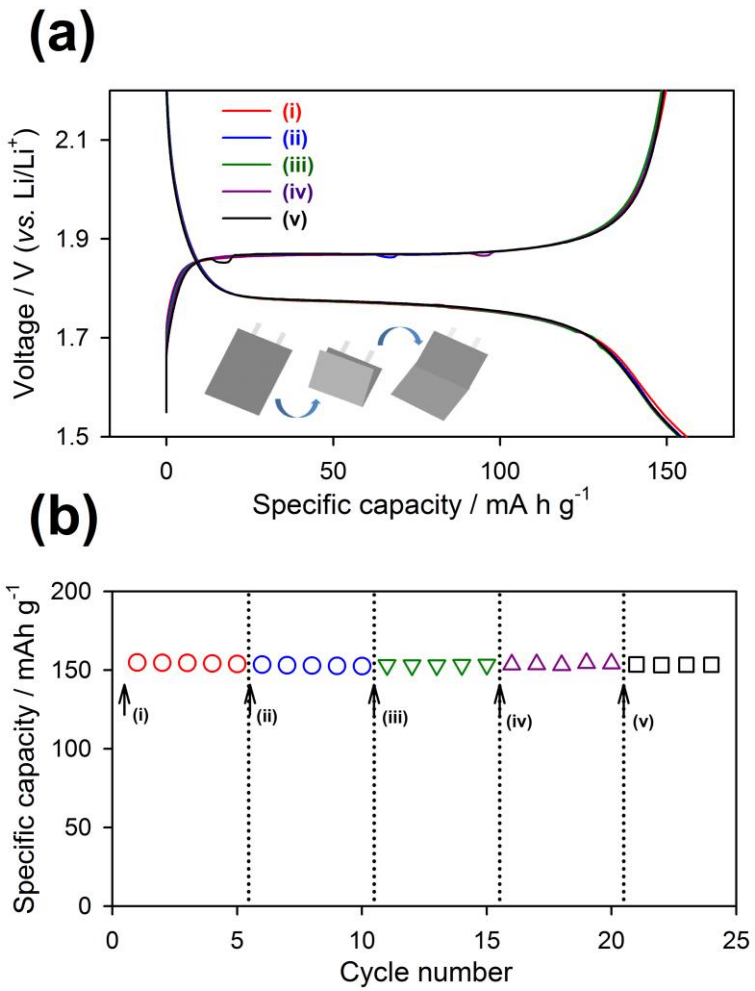


**Figure 29.** (a); Voltage profile of Li/$TiO_2$-deposited SUS fabric cell (pouch-type) before and after folding test. One fold means a cycle of folding and unfolding. Cycle retention is presented in (b). Each folding test, consisting of 30 folds, was conducted at the end of every five electrochemical cycles ((ii), (iii), (iv), and (v)). The schematic diagram of one fold is shown in the inset of (a).

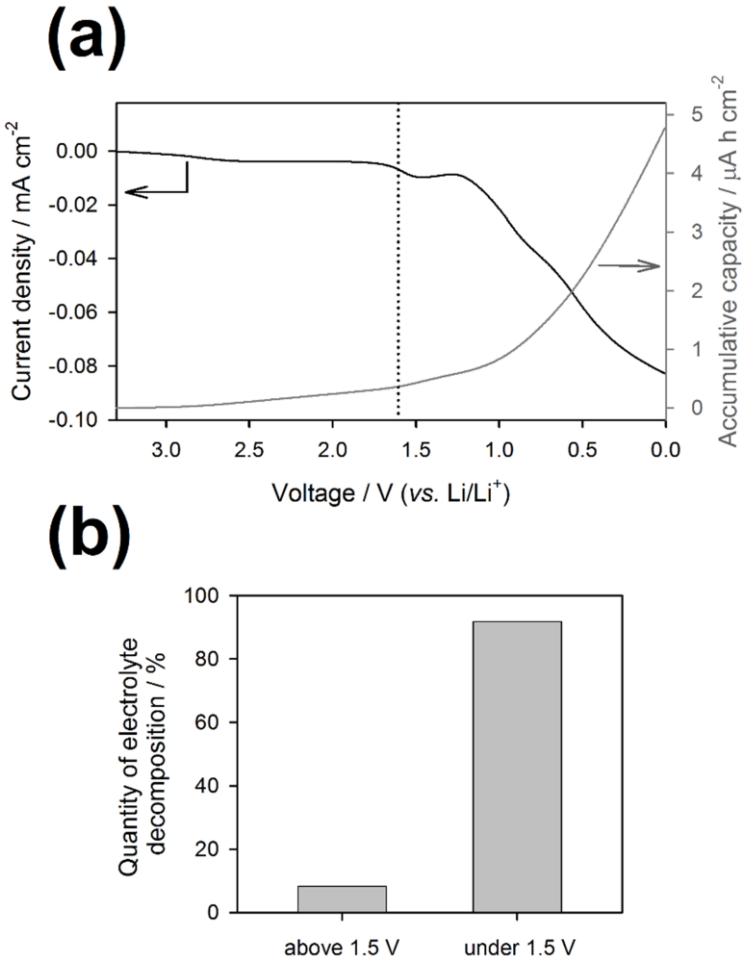


**Figure 30.** (a); the data of linear sweep voltammetry using Cu electrode. Voltage was swept from OCV to 0 V (*vs.* $Li/Li^+$). (b); the calculation result of electrolyte decomposition, which was based on linear sweep voltammetry data.

### 3.2.6. High power negative electrode by 3-dimensionally well-constructed SUS fabric

SUS fabric provides a 3-dimensionally well-developed electric path as a current collector. The conventional electrode is composed of electrode layer and current collector, and they are separated layer-by-layer. Usually, electrode layer is made up by active material, binder and conducting agent. In this case, the active material located in top-most of electrode layer is apart from the current collector. Thus, conducting agent is added to electrode component to provide a sufficient electric path between active material and current collector. When SUS fabric is used as a current collector, current collector is not separated from electrode layer, and it is uniformly distributed in electrode layer. Active material and current collector are close each other, and there is no use for conducting agent. As a result, the electrode has a better electric path over the whole electrode than the conventionally fabricated electrode, which uses Cu foil as a current collector. It is attributed to a SUS fabric current collector, which is categorized as a metal and has a superior electric conductivity than the conventionally used conducting agent, such as a carbon.

Active material is deposited on SUS fabric as a thin film. Thus, the overall morphology of the electrode depends on the structure of SUS fabric (Figure 31). The void spaces at the inner part of SUS fabric is maintained even after active material loading, and this trait helps electrolyte containing lithium-ion easily contact soak into the electrode. As a result, the contact area between active material and electrolyte becomes large. And, the lithium transfer between active material and current collector becomes easy. Also, the rest time, which is essential for electrolyte to penetrate into electrode before the electrochemical cycling, could be shortened.

The rate capability of electrode depends on both lithium-ion conductivity and electric conductivity. Then, the electrode utilized SUS fabric as a current collector provides not only better electric path but also more efficient lithium-ion path than the conventionally fabricated

electrode. Thus, it is easily expected that the rate capability of the electrode from SUS fabric is better than that of the conventional electrode. In this chapter, it is examined whether the electrode using SUS fabric as a current collector shows a better rate capability than the conventional electrode, and it is explained what the reason is for increase in rate capability.

For this purpose, control group and comparison group are selected as follows (Table 7). The current collector of control group is SUS fabric, and $TiO_2$ is deposited onto SUS fabric as an active material by liquid-phase deposition. In other words, $TiO_2$-deposited SUS fabric is a control group. The current collector of comparison group is Cu foil, and $TiO_2$ is coated onto Cu foil as an active material by the conventional slurry spreading method. The electrode layer is composed of $TiO_2$ powder as an active material, PVdF binder and carbon black as a conducting agent. They are in weight ratio of 90:5:5. $TiO_2$ powder is recollected during liquid-phase deposition. That is, $TiO_2$-coated Cu foil is a comparison group. The loading lever of active material is similar in two electrodes as about 1 mg $cm^{-2}$, and the amount of binder and conducting agent in comparison group is minimized. Two electrodes uses in same kinds of active material, and there is a major difference in current collector. Thus, when the rate capability is different in two electrodes, the major reason must be traced from current collector.

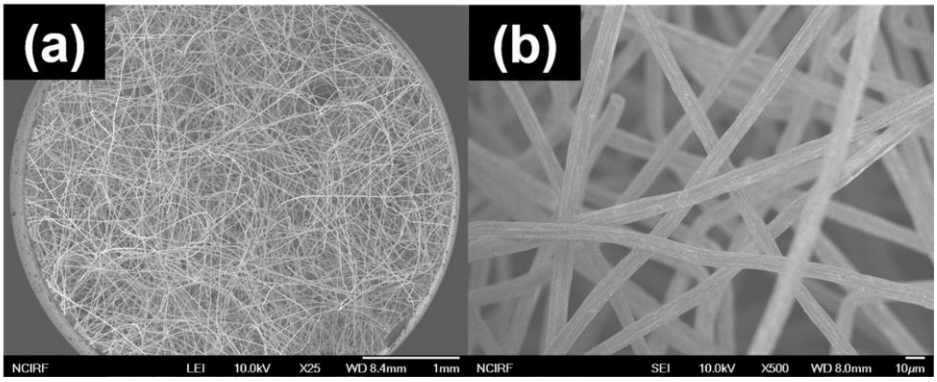


**Figure 31.** FE-SEM images of SUS fabric current collector. (b) is a magnified image of (a).

**Table 7.** The specification of control group and comparison group.

| | **Control group** | **Comparison group** |
|---|---|---|
| Active material | Deposited $TiO_2$ | Precipitated $TiO_2$ |
| Binder | X | PVdF (5 *wt.*%) |
| Conducting agent | X | Carbon black (5 *wt.*%) |
| Current collector | SUS fabric | Cu foil |

The phase of active material is checked by Raman spectroscopy (Figure 32). The upper graph is about SUS fabric only, and the middle graph is about $TiO_2$-deposited SUS fabric. When $TiO_2$ is deposited onto SUS fabric, additional peaks are seen at 395, 516 and 640 $cm^{-1}$. These peaks are well-matched with that of anatase $TiO_2$. Thus, it could be inferred that the phase of deposit is almost anatase $TiO_2$. The lower graph is related with $TiO_2$ powder recollected during liquid-phase deposition. Also, unique peaks of anatase $TiO_2$ are well shown in the graph. It can be concluded that there is no difference in the kinds of active material between control group and comparison group.

The phase of active material used in two electrodes can also be confirmed by electrochemical analysis methods (Figure 33). In the case of control group, it shows voltage plateau of lithium-reaction at around 1.8 V (*vs.* $Li/Li^+$), and delivers the specific capacity as 162 mA h $g^{-1}$ (Figure 33a). These traits are completely identical with typical anatase $TiO_2$. In the case of comparison group, it shows a little bit smaller specific capacity (145 mA h $g^{-1}$) than typical anatase $TiO_2$ by the usual electrochemical cycling condition. Thus, EVS test was conducted to grasp the maximum reversible capacity and the thermodynamic data of comparison group. As a result, the de-lithiation voltage plateau is revealed at 1.8 V (*vs.* $Li/Li^+$), and the electrode shows its reversible capacity as 165 mA h $g^{-1}$ (Figure 33b). Therefore, it can be illuminated that the electrochemically same kind of active material is used to fabricate two electrodes, and the phase of active material is anatase $TiO_2$.

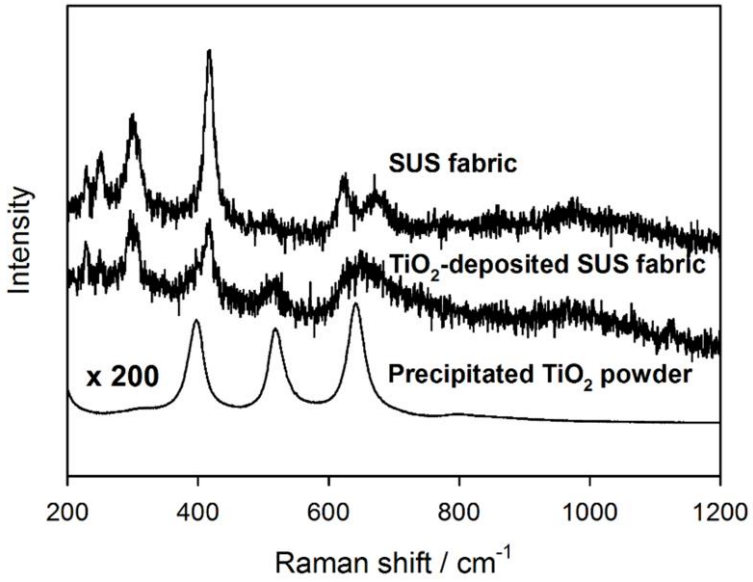


**Figure 32.** Raman data of SUS fabric, $TiO_2$-deposited SUS fabric by liquid-phase deposition method and recollected $TiO_2$ powder during liquid-phase deposition.

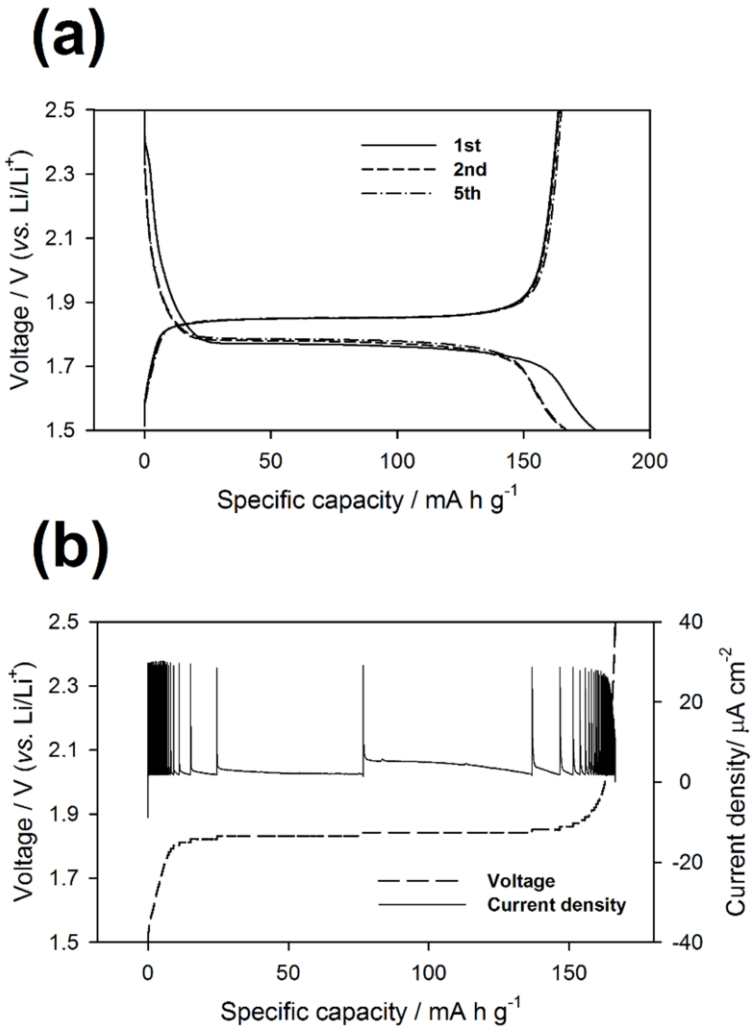


**Figure 33.** (a); voltage profile of $TiO_2$-deposited SUS fabric electrode (control group). (b); EVS data of $TiO_2$-coated Cu foil electrode (comparison group).

Rate capability is compared in two electrodes by the electrochemical analysis method (Figure 34). The condition of voltage cut-off is from 1.5 V (*vs.* $Li/Li^+$) to 2.5 V (*vs.* $Li/Li^+$), and the voltage plateau of lithium reaction is around 1.8 V (*vs.* $Li/Li^+$), which is near the lower voltage cut-off. Thus, rate test is conducted only by changing the current density of delithiation. As a result, the electrode of control group showed a better rate capability than the electrode of comparison group. Especially, the capacity retention of $TiO_2$-coated Cu foil electrode is almost zero at 10 C-rate, while that of $TiO_2$-deposited SUS fabric electrode maintains about 80 %. Therefore, it can be concluded that the rate capability of $TiO_2$-deposited SUS fabric electrode is superior than that of $TiO_2$-coated Cu foil electrode.

GITT test was conducted to trace the reason for difference in rate capability (Figure 35). According to the data, the internal resistance of $TiO_2$-deposited SUS fabric electrode is lower over whole voltage range than that of $TiO_2$-coated Cu foil electrode. Especially, there are drastic difference during de-lithiation. It means that during electrochemical cycling, control group feels lower overpotential than comparison group. And, during electrochemical cycling, $TiO_2$-coated Cu foil electrode reaches voltage cut-off faster than $TiO_2$-deposited SUS fabric electrode. Thus it can be inferred that the better rate capability in control group is attributed to the lower internal resistance. However, the fundamental reason for difference in rate capability cannot be explained only by GITT test. Thus, EIS test must be followed to figure out the basic reason for difference in rate capability.

EIS test was conducted to trace the basic reason for difference in rate capability (Figure 36). Black graph is about $TiO_2$-deposited SUS fabric electrode and grey graph is about $TiO_2$-coated Cu foil electrode. The electrodes were electrochemically cycled fully one time, and the state of charge (SOC) was maintained to be 50. The test condition is from 1 mHz to 100 kHz. The respective graphs are composed of two semicircles, and the amount of resistance is reflected on the size of semicircle. The semicircle near the origin point shows the resistance related with

solid-electrolyte interphase (SEI), and the other, which is far from the origin point, means the resistance of charge transfer. The size of two semicircles are smaller in control group than in comparison group. To figure out the size of the resistance quantitatively, fitting process was followed. According to the data, resistances are smaller in control group, and especially, charge transfer resistance shows a major difference. Charge transfer resistance means the resistance for mass transfer into active material, such as lithium-ion and electron. Because two electrodes utilize the same kind of active material and electrolyte, there is an only difference in current collector. There are two main reasons for improvement in charge transfer resistance, and they are explained in detail.

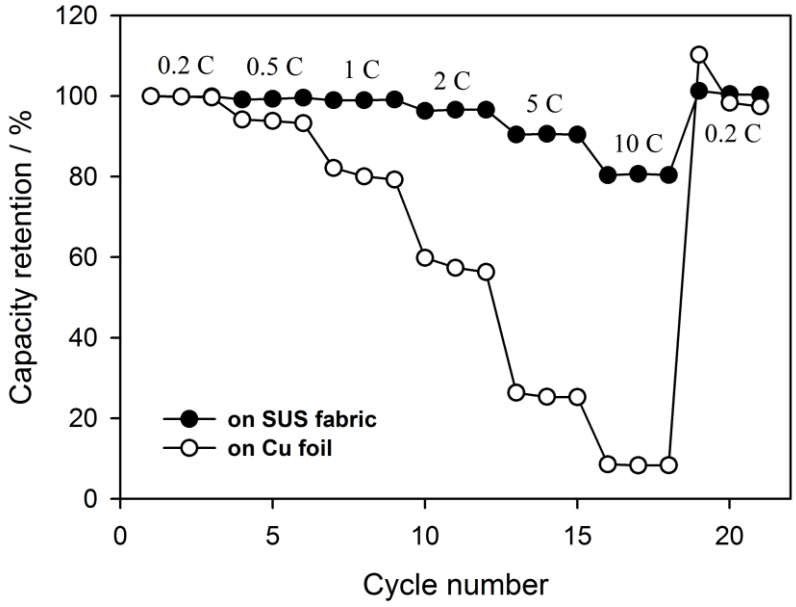


**Figure 34.** The rate capability data of two electrodes. Only delithiation rate was varied from 0.2 C-rate to 10 C-rate.

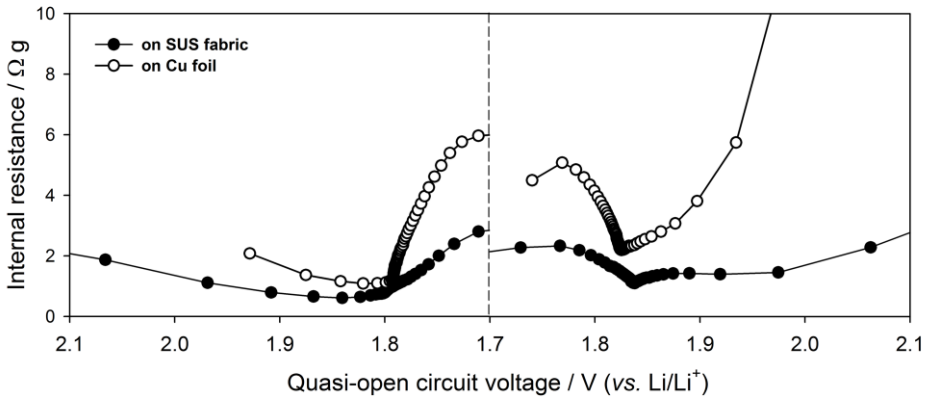


**Figure 35.** The GITT data of two electrodes. Internal resistance was calculated from imposed current and voltage drop. Voltage drop is based on the difference between CCV and QOCV.

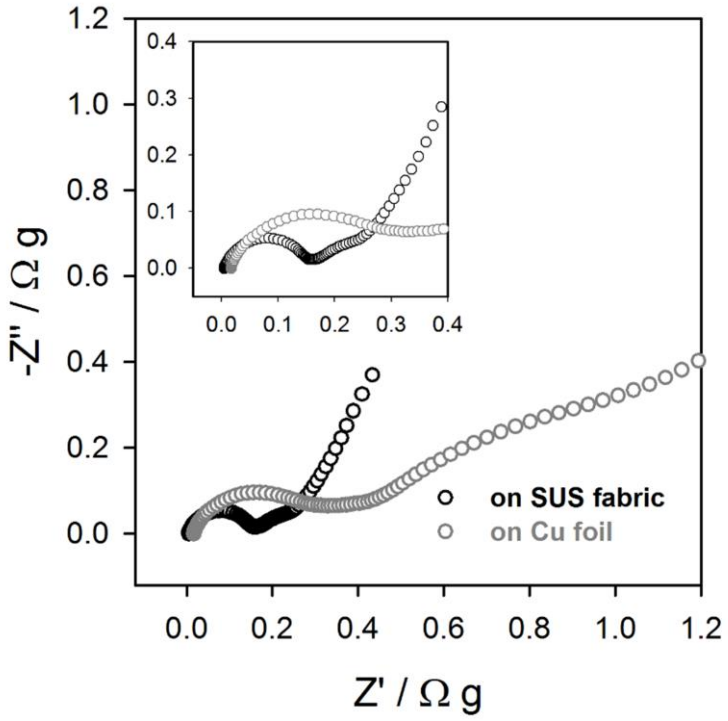


**Figure 36.** The EIS results of two electrodes. The test was conducted at SOC 50 after 1st electrochemical cycling. Inset: a magnified data to figure out two semicircles of $TiO_2$-deposited SUS fabric electrode (control group).

Firstly, the structure of current collector can be suggested. The typical structure of conventionally fabricated electrode can be described as follows (Figure 2). In the conventional electrode, the current collector is separated with the electrode layer. The electrode layer is constituted by active material, binder and conducting agent. Current collector provides the electric path from electrode layer to external circuit, and conducting agent gives the electric path through electrode layer. Thus, electron transfer in the electrode layer of conventional electrode is mainly conducted by conducting agent. On the other hand, the structure of $TiO_2$-deposited SUS fabric electrode can be depicted as follows (Figure 37). In this electrode, current collector is uniformly distributed over the electrode layer. And, SUS fabric provides 3-dimensionally well-distributed electric network. Thus, electron transfer in the electrode layer of $TiO_2$-deposited SUS fabric electrode is mainly conducted by current collector.

The electric conductivity of several material can be checked as follows. Among the material candidates of current collector, electric conductivity of copper is the best ($5.96 * 10^7$ S $m^{-1}$), and that of SUS is second ($1.45 * 10^6$ S $m^{-1}$), and that of carbon is the last ($1.25 * 10^3$ S $m^{-1}$). In $TiO_2$-deposited SUS fabric electrode, the material which helps the conduction of electron is SUS. And, in $TiO_2$-coated Cu foil electrode, the material which helps the conduction of electron is carbon. Thus, in control group, electron transfer through the electrode layer is faster than in comparison group. It makes the rate capability of control group be better, and makes an effect on charge transfer resistance during EIS test. These effects comes from the unique structure of SUS fabric current collector.

The effect from SUS fabric's unique structure can be understood by analogous experiment. SUS fabric has the larger surface area than Cu foil. Thus, when the similar amount of active material are loaded onto SUS fabric and Cu foil respectively, the thickness of loaded material is thinner in SUS fabric than in Cu foil. Thus, it is true that the thickness of electrode layer becomes thin by using SUS fabric as a current collector. To evaluate the effect of the thickness of electrode layer

on the electrochemical property, various electrodes are prepared which are only different in thickness each other. As a result, when the thickness of electrode gets thinner, the polarization becomes smaller. And, also the thickness of electrode influences the specific capacity of prepared electrode. In other words, by adopting SUS fabric as a current collector, the thickness of electrode layer is decreased, and the electrochemical properties get better.

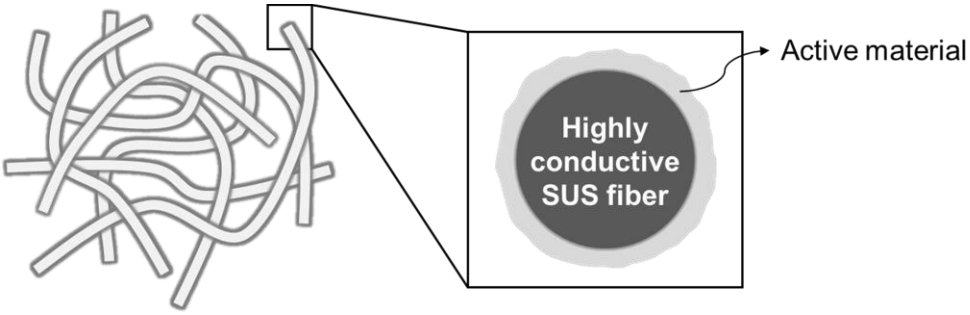


**Figure 37.** Basic design for electrode components of $TiO_2$-deposited SUS fabric.

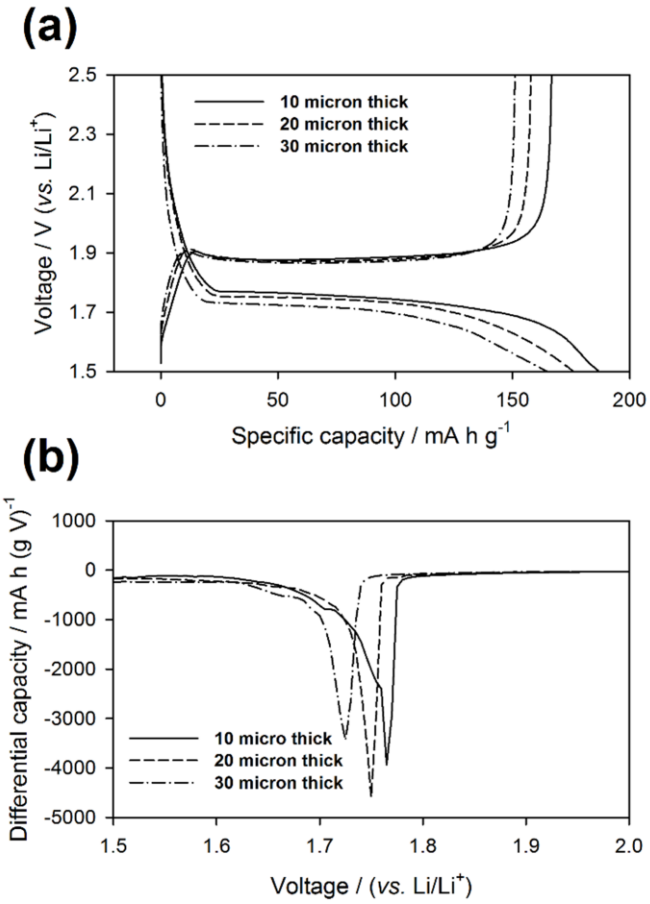


**Figure 38.** (a); Voltage profile of $TiO_2$-deposited SUS fabric electrodes with the various electrode layer thickness. (b); The differential capacity plot of $TiO_2$-deposited SUS fabric electrodes with the various electrode layer thickness.

Secondly, the surface area of electrode can be suggested. It is expected that when SUS fabric is used as a current collector, the surface area of electrode could be increased, compared with the case of Cu foil current collector. Because the shape of electrode is controlled by the shape of current collector, it seems to be true. However, we must consider the exact meaning of the surface area of electrode. The surface area of electrode means the contact area between active material and electrolyte. This area could be similar between $TiO_2$-deposited SUS fabric electrode and $TiO_2$-coated Cu foil electrode which use same kinds of active material. In other words, when two electrodes use same kinds of active material, they shows a similar degree of the surface area, although they uses in different kinds of current collector.

However, in fact, the surface area of control group could be smaller than that of comparison group. In the case of Cu foil current collector, it has a smaller surface area than that of SUS fabric current collector. Thus, when the same amount of active material is loaded onto current collector, the thickness of electrode layer must be thicker on Cu foil than SUS fabric. In this situation, the migration of electrolyte could be hindered through thick electrode layer. In fact, the contact area between active material and electrolyte could be decreased, compared with the total amount from respective area of active material. Also, there is an additional reason for decrease in surface area of electrode. In the case of control group, active material is loaded onto SUS fabric by liquid-phase deposition method. In this process, there is no use in binder. On contrary, PVdF is utilized as a binder in comparison group. Binder is coated onto the surface of active material, and grant the adhesion strength among active material and current collector. In this process, the contact area between active material and electrolyte can be decreased. In fact, this effect from binder can be checked, as seen in Figure 39.

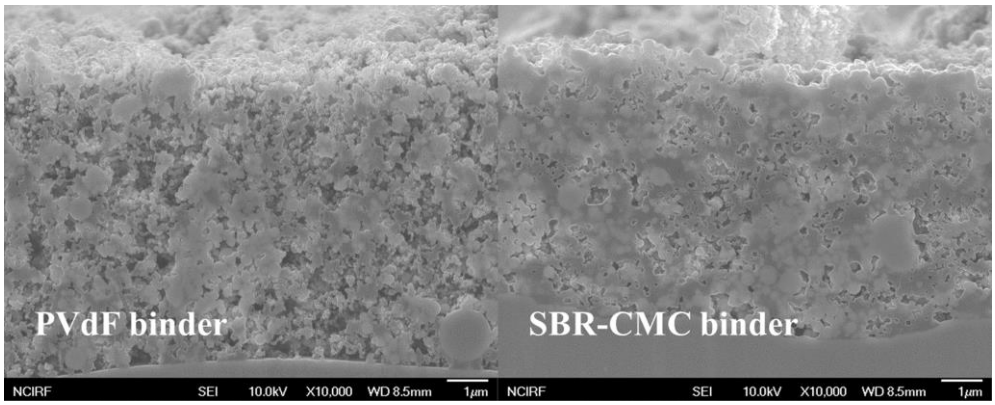


**Figure 39.** The cross-sectional images of $TiO_2$-coated Cu foil electrode. The electrode is composed of $TiO_2$ active material, binder and super P conducting agent. The electrode from left image uses PVdF binder, and the electrode from right image uses SBR-CMC binder.

Now, to quantify the decrease in surface area of electrode, cyclic voltammetry experiment was conducted, using $TiO_2$-deposited SUS fabric electrode and $TiO_2$-coated Cu foil electrode. Voltage sweep was conducted from 2.0 V (*vs.* $Li/Li^+$) to 2.5 V (*vs.* $Li/Li^+$) in which only non-faradaic reaction takes place. In two electrode, capacitance is similar, because they use the same kinds of active material. Thus, the contact area between active material and electrolyte could be compared from the maximum current density during cyclic voltammetry experiment. Current density was amended by the weight of active material.

As seen in Figure 40, when SUS fabric is utilized as a current collector, the maximum current density is bigger than that from Cu foil. In other words, the surface area of electrode depends on structure of current collector and way for preparing active material. When cyclic voltammetry was conducted with various scan rate, the slope of $TiO_2$-deposited SUS fabric electrode is 3-times steeper than that of $TiO_2$-coated Cu foil electrode. Thus, lithium transfer between active material and electrolyte could be easy by 3-times large surface area of $TiO_2$-deposited SUS fabric electrode. This effect have an effect on rate capability and charge transfer resistance during EIS experiment.

The reason for better rate capability of TiO2-coated SUS fabric electrode is analyzed by various experiment. When SUS fabric is used as a current collector, 3-dimensionally well-connected network helps the electronic flow over the whole electrode. As mentioned before, when SUS fabric is used, active material is not far from SUS fabric, because the SUS fabric is uniformly distributed over the whole electrode. Thus, it is reasonable that the kind of current collector makes the difference in the ability related with electron transfer, and it is a first reason for the superior rate capability in $TiO_2$-deposited SUS fabric electrode. Also, when SUS fabric is used as a current collector, the surface area of electrode is large, and lithium-transfer between active material and electrolyte is easy. There is a difference in the ability related with lithium transfer, and it is a second reason for the superior rate capability in $TiO_2$-deposited SUS fabric electrode.

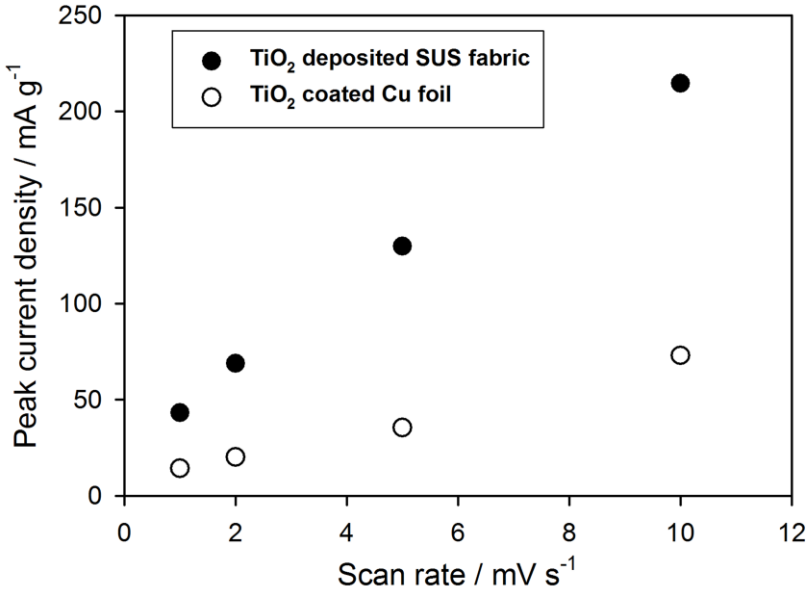


**Figure 40.** The cyclic voltammetry result of two electrodes. The peak current density was collected with various scan rate condition.

### 3.2.7. Summary of section

In this research, SUS fabric was utilized as a current collector of negative electrode of lithium-ion batteries. SUS shows a property of free-standing and highly electric conducting, which are essential properties as a current collector. Furthermore, unique properties of the used current collector makes the electrode distinguishable from the conventionally fabricated electrode. It is possible to develop a new type of negative electrode, such as a flexible and high rate capability negative electrode.

$TiO_2$-deposited SUS fabric prepared as the negative electrode has the following three primary characteristics. The stress generated during a flexibility test dissipated effectively on the 3-dimensional structured SUS fabric, which constructs the backbone of electrode as a current collector. Also, strong adhesion strength is retained at the interface between the active material and the current collector via liquid-phase deposition. Finally, the material selection of $TiO_2$ makes the maintenance of the initial adhesion strength possible. We attributed this to the characteristic of $TiO_2$, which undergoes negligible volume change during electrochemical cycling.

The prepared electrode could fulfill the requirements as a flexible electrode based on these listed characteristics. This is supported by the following results of the folding test. There is no detachment of the active material from the current collector. And, the imposed stress has no effect on electrochemical properties such as specific capacity, polarization, and cycle retention.

Also, the $TiO_2$-deposited SUS fabric prepared as the negative electrode has the additional characteristics. SUS fabric has a well-constructed 3-dimensional electric path, and large pore size at the inner space to migrate electrolyte smoothly. When the SUS fabric is used as a current collector, it is expected for the fabricated electrode to show a high rate capability. In fact, the control group shows a better rate capability. And, the well-constructed electric path and large

surface area of electrode is the major reason for the better rate capability of control group. Therefore, the use of SUS fabric to compose flexible and high rate lithium-ion batteries worthy of further investigation.

# Chapter 4. CONCLUSIONS

The conventional research for negative electrode has been focused on active material among the components of electrode, because, active material plays an important role in negative electrode to decide abilities about the specific capacity, rate capability and cycleability. Many researchers have reported that the advanced electrode can be developed by search of the novel active material and surface modification of active material. Also, many researches have been concentrated on binder. Binder provides an adhesion strength among active material and current collector. When the binder of strong adhesion strength is used to construct a negative electrode, the detachment of active material during electrochemical cycling is prevented. In these days, active materials, which show the high specific capacity an experience large volume change, are utilized, thus binder, which provides strong adhesion strength, must be developed to deliver the capacity of active material stably.

In this research, new approach is suggested to develop the advanced negative electrode. Strategy is focused on current collector, and negative electrodes with advanced and unique properties are developed by improvement in current collector. Firstly, the negative electrode of high specific capacity is manufactured by carbon fabric current collector. It is attributed to the property of carbon fabric, which has a reactivity with lithium ion at working voltage range. Secondly, the negative electrode of flexible and high rate capability is constructed by SUS fabric current collector. It comes from the property of SUS fabric, which is flexible and highly electric conducting.

In this research, new prospect is suggested to develop the desirable negative electrodes. The improvement in active material is on the state of saturation. There has been already many kinds

of research on active material. In this state, current collector must be researched and modified to overcome the limitation and develop the advanced negative electrode for lithium-ion batteries. Especially, current collector rules the shape of electrode, and it makes the research on current collector fascinating. Without any change in active material, the negative electrode with desired properties can be developed by using materially and structurally unique current collector.

# References

[1] B. Scrosati, Electrochimica Acta 45 (2000) 2461-2466.

[2] J.M. Tarascon, M. Armand, Nature 414 (2001) 359-367.

[3] H. Chen, T.N. Cong, W. Yang, C. Tan, Y. Li, Y. Ding, Progress in Natural Science 19 (2009) 291-312.

[4] V. Etacheri, R. Marom, R. Elazari, G. Salitra, D. Aurbach, Energ Environ Sci 4 (2011) 3243-3262.

[5] M.M. Thackeray, C. Wolverton, E.D. Isaacs, Energ Environ Sci 5 (2012) 7854-7863.

[6] L. Lu, X. Han, J. Li, J. Hua, M. Ouyang, Journal of Power Sources 226 (2013) 272-288.

[7] K. Kang, Y.S. Meng, J. Bréger, C.P. Grey, G. Ceder, Science 311 (2006) 977-980.

[8] H.-W. Lee, P. Muralidharan, R. Ruffo, C.M. Mari, Y. Cui, D.K. Kim, Nano Lett 10 (2010) 3852-3856.

[9] C. Sun, S. Rajasekhara, J.B. Goodenough, F. Zhou, Journal of the American Chemical Society 133 (2011) 2132-2135.

[10] C.K. Chan, X.F. Zhang, Y. Cui, Nano Lett 8 (2008) 307-309.

[11] E. Yoo, J. Kim, E. Hosono, H.-s. Zhou, T. Kudo, I. Honma, Nano Lett 8 (2008) 2277-2282.

[12] L.-F. Cui, Y. Yang, C.-M. Hsu, Y. Cui, Nano Lett 9 (2009) 3370-3374.

[13] L. Hu, H. Wu, F. La Mantia, Y. Yang, Y. Cui, ACS Nano 4 (2010) 5843-5848.

[14] B. Liu, J. Zhang, X. Wang, G. Chen, D. Chen, C. Zhou, G. Shen, Nano Lett 12 (2012) 3005-3011.

[15] S.-Y. Lee, K.-H. Choi, W.-S. Choi, Y.H. Kwon, H.-R. Jung, H.-C. Shin, J.Y. Kim, Energ Environ Sci 6 (2013) 2414-2423.

[16] K.M. Abraham, Electrochimica Acta 38 (1993) 1233-1248.

[17] B.J. Neudecker, N.J. Dudney, J.B. Bates, J Electrochem Soc 147 (2000) 517-523.

[18] D. Aurbach, Y. Talyosef, B. Markovsky, E. Markevich, E. Zinigrad, L. Asraf, J.S. Gnanaraj, H.-J. Kim, Electrochimica Acta 50 (2004) 247-254.

[19] R. Marom, S.F. Amalraj, N. Leifer, D. Jacob, D. Aurbach, J Mater Chem 21 (2011) 9938-9954.

[20] M.B. Armand, Intercalation Electrodes, in: D.W. Murphy, J. Broadhead, B.C.H. Steele (Eds.) Materials for Advanced Batteries, Springer US, Boston, MA, 1980, pp. 145-161.

[21] B. Scrosati, J Electrochem Soc 139 (1992) 2776-2781.

[22] X. Ji, K.T. Lee, L.F. Nazar, Nat Mater 8 (2009) 500-506.

[23] G. Girishkumar, B. McCloskey, A.C. Luntz, S. Swanson, W. Wilcke, The Journal of Physical Chemistry Letters 1 (2010) 2193-2203.

[24] H. Wang, Y. Yang, Y. Liang, J.T. Robinson, Y. Li, A. Jackson, Y. Cui, H. Dai, Nano Lett 11 (2011) 2644-2647.

[25] H.-G. Jung, J. Hassoun, J.-B. Park, Y.-K. Sun, B. Scrosati, Nat Chem 4 (2012) 579-585.

[26] Z. Peng, S.A. Freunberger, Y. Chen, P.G. Bruce, Science 337 (2012) 563-566.

[27] J.R. Dahn, T. Zheng, Y.H. Liu, J.S. Xue, Science 270 (1995) 590-593.

[28] D. Aurbach, B. Markovsky, I. Weissman, E. Levi, Y. Ein-Eli, Electrochimica Acta 45 (1999) 67-86.

[29] K. Mizushima, P.C. Jones, P.J. Wiseman, J.B. Goodenough, Materials Research Bulletin 15 (1980) 783-789.

[30] J.W. Fergus, Journal of Power Sources 195 (2010) 939-954.

[31] D. Aurbach, B. Markovsky, G. Salitra, E. Markevich, Y. Talyossef, M. Koltypin, L. Nazar, B. Ellis, D. Kovacheva, Journal of Power Sources 165 (2007) 491-499.

[32] K.X. Liumin Suo, et al., Science 350 (2015).

[33] S.S. Zhang, Journal of Power Sources 164 (2007) 351-364.

[34] J. Li, R.B. Lewis, J.R. Dahn, Electrochemical and Solid-State Letters 10 (2007) A17-A20.

[35] J. Li, D.-B. Le, P.P. Ferguson, J.R. Dahn, Electrochimica Acta 55 (2010) 2991-2995.

[36] F. Ding, W. Xu, X.L. Chen, J. Zhang, M.H. Engelhard, Y.H. Zhang, B.R. Johnson, J.V. Crum, T.A. Blake, X.J. Liu, J.G. Zhang, J Electrochem Soc 160 (2013) A1894-A1901.

[37] F. Orsini, A. Du Pasquier, B. Beaudoin, J.M. Tarascon, M. Trentin, N. Langenhuizen, E. De Beer, P. Notten, Journal of Power Sources 76 (1998) 19-29.

[38] F. Orsini, A. du Pasquier, B. Beaudouin, J.M. Tarascon, M. Trentin, N. Langenhuizen, E. de Beer, P. Notten, Journal of Power Sources 81 (1999) 918-921.

[39] S.K. Kong, B.K. Kim, W.Y. Yoon, J Electrochem Soc 159 (2012) A1551-A1553.

[40] J.G. Kim, B. Son, S. Mukherjee, N. Schuppert, A. Bates, O. Kwon, M.J. Choi, H.Y. Chung, S. Park, Journal of Power Sources 282 (2015) 299-322.

[41] G. Tan, F. Wu, C. Zhan, J. Wang, D. Mu, J. Lu, K. Amine, Nano Lett 16 (2016) 1960-1968.

[42] T. Zheng, J.N. Reimers, J.R. Dahn, Phys Rev B 51 (1995) 734-741.

[43] W.-J. Zhang, Journal of Power Sources 196 (2011) 13-24.

[44] M.N. Obrovac, L. Christensen, D.B. Le, J.R. Dahnb, J Electrochem Soc 154 (2007) A849-A855.

[45] N. Dimov, S. Kugino, M. Yoshio, Electrochimica Acta 48 (2003) 1579-1587.

[46] F. Cao, I.V. Barsukov, H.J. Bang, P. Zaleski, J. Prakash, J Electrochem Soc 147 (2000) 3579-3583.

[47] P. Arora, R.E. White, M. Doyle, J Electrochem Soc 145 (1998) 3647-3667.

[48] H. Kim, M. Seo, M.H. Park, J. Cho, Angew Chem Int Edit 49 (2010) 2146-2149.

[49] K.D. Kepler, J.T. Vaughey, M.M. Thackeray, Electrochem Solid St 2 (1999) 307-309.

[50] D. Larcher, L.Y. Beaulieu, D.D. MacNeil, J.R. Dahn, J Electrochem Soc 147 (2000) 1658-1662.

[51] L.B. Chen, K. Wang, X.H. Xie, J.Y. Xie, Journal of Power Sources 174 (2007) 538-543.

[52] V. Etacheri, O. Haik, Y. Goffer, G.A. Roberts, I.C. Stefan, R. Fasching, D. Aurbach, Langmuir 28 (2012) 965-976.

[53] S.Y. Huang, L. Kavan, I. Exnar, M. Grätzel, J Electrochem Soc 142 (1995) L142-L144.

[54] J.H. Yao, T. Takasaki, K. Nishimura, T. Mukai, T. Sakai, J Electrochem Soc 160 (2013) A980-A984.

[55] H. Pizem, C.N. Sukenik, U. Sampathkumaran, A.K. McIlwain, M.R. De Guire, Chem Mater 14 (2002) 2476-2485.

[56] D.W. Dees, S. Kawauchi, D.P. Abraham, J. Prakash, Journal of Power Sources 189 (2009) 263-268.

[57] J.H. Ryu, J.W. Kim, Y.-E. Sung, S.M. Oh, Electrochemical and Solid-State Letters 7 (2004) A306-A309.

[58] C.W. Park, S.-H. Yoon, S.M. Oh, Carbon 38 (2000) 1261-1269.

[59] B. Scrosati, J. Garche, Journal of Power Sources 195 (2010) 2419-2430.

[60] Y. Idota, T. Kubota, A. Matsufuji, Y. Maekawa, T. Miyasaka, Science 276 (1997) 1395-1397.

[61] A. Ulus, Y. Rosenberg, L. Burstein, E. Peled, J Electrochem Soc 149 (2002) A635-A643.

[62] J.H. Ku, J.H. Ryu, S.H. Kim, O.H. Han, S.M. Oh, Adv Funct Mater 22 (2012) 3658-3664.

[63] Y. Park, N.-S. Choi, S. Park, S.H. Woo, S. Sim, B.Y. Jang, S.M. Oh, S. Park, J. Cho, K.T. Lee, Advanced Energy Materials 3 (2013) 206-212.

[64] B.M. Bang, J.-I. Lee, H. Kim, J. Cho, S. Park, Advanced Energy Materials 2 (2012) 878-883.

[65] E. Peled, C. Menachem, D. Bar-Tow, A. Melman, J Electrochem Soc 143 (1996) L4-L7.

[66] S.-K. Jeong, M. Inaba, R. Mogi, Y. Iriyama, T. Abe, Z. Ogumi, Langmuir 17 (2001) 8281-8286.

[67] H.C. Shin, M.L. Liu, Adv Funct Mater 15 (2005) 582-586.

[68] H.B. Zhang, Y.H. Ye, R.Q. Shen, C.B. Ru, Y. Hu, J Electrochem Soc 160 (2013) D441-D445.

[69] L. Yue, W.H. Zhang, J.F. Yang, L.Z. Zhang, Electrochimica Acta 125 (2014) 206-217.

[70] M. Manickam, M. Takata, Electrochimica Acta 48 (2003) 957-963.

[71] H. Buqa, M. Holzapfel, F. Krumeich, C. Veit, P. Novák, Journal of Power Sources 161 (2006) 617-622.

[72] B. Scrosati, Nat Nano 2 (2007) 598-599.

[73] H. Nishide, K. Oyaizu, Science 319 (2008) 737-738.

[74] L.-F. Chen, Z.-H. Huang, H.-W. Liang, W.-T. Yao, Z.-Y. Yu, S.-H. Yu, Energ Environ Sci 6 (2013) 3331-3338.

[75] X.H. Wang, C. Guan, L.M. Sun, R.A. Susantyoko, H.J. Fan, Q. Zhang, J Mater Chem A 3 (2015) 15394-15398.

[76] M. Park, D. Lee, S. Shin, H.-J. Kim, J. Hyun, Carbohydrate Polymers 140 (2016) 43-50.

[77] M. Lee, J. Hong, H. Kim, H.D. Lim, S.B. Cho, K. Kang, C.B. Park, Adv Mater 26 (2014) 2558-2565.

[78] J.W. Hu, Z.P. Wu, S.W. Zhong, W.B. Zhang, S. Suresh, A. Mehta, N. Koratkar, Carbon 87 (2015) 292-298.

[79] J.S. Chou, S.C. Lee, J Electrochem Soc 141 (1994) 3214-3218.

[80] B. Herbig, P. Löbmann, Journal of Photochemistry and Photobiology A: Chemistry 163 (2004) 359-365.

[81] Z. Liuxue, W. Xiulian, L. Peng, S. Zhixing, Surface and Coatings Technology 201 (2007) 7607-7614.

[82] J. Kim, J. Cho, J Electrochem Soc 154 (2007) A542-A546.

[83] C.X. Lei, H. Zhou, Z.D. Feng, Y.F. Zhu, R.G. Du, Appl Surf Sci 257 (2011) 7330-7334.

[84] C.T. Cherian, M.V. Reddy, T. Magdaleno, C.H. Sow, K.V. Ramanujachary, G.V.S. Rao,

B.V.R. Chowdari, Crystengcomm 14 (2012) 978-986.

[85] J.S. Kim, Y.H. Lee, I. Lee, T.S. Kim, M.H. Ryou, J.W. Choi, J Mater Chem A 2 (2014) 10862-10868.

[86] G. Sudant, E. Baudrin, D. Larcher, J.M. Tarascon, J Mater Chem 15 (2005) 1263-1269.

# 요약 (국문초록)

음극은 활물질과 바인더, 도전재, 그리고 집전체로 구성된다. 본 연구에서는 물질적 구조적으로 특수한 집전체 활용을 통해 전극의 성능을 개선시키고자 한다. 탄소 부직포와 SUS 부직포를 이용하여 실험을 진행하였는데, 탄소 부직포를 통해 고용량 음극을, SUS 부직포를 통해서는 휨 특성이 좋고 속도 특성이 뛰어난 음극을 개발하였다.

고용량 음극을 개발하기 위해 $Cu_6Sn_5$ alloy가 코팅된 탄소 부직포를 성공적으로 제작하였다. 흑연은 높은 전기전도도를 갖는 물질로 잘 알려졌으며, 집전체로 충분히 활용 가능하다. 만약 흑연을 집전체로 사용한다면, 집전체는 기존의 그것처럼 전기전도 경로를 제공할 뿐 아니라, 또한 리튬 이온과 전기화학적인 반응을 하면서 추가적인 용량을 발현한다. 본 연구에서는, 전극의 용량을 증진시키기 위해 탄소 부직포를 집전체로 활용하여 전극을 구성했다. 활물질로 선택된 $Cu_6Sn_5$의 경우에는 전기화학적인 충방전 과정 중에 집전체로부터의 탈리가 발견되지 않았다. 즉, 안정적인 수명특성을 보였다. 결과적으로, 전체 전극의 무게를 이용하여 무게당 용량을 계산하였을 때, 약 300 $mA\,h\,g^{-1}$ 정도의 용량을 안정적으로 발현하는 전극을 개발할 수 있었다. 이 값은 구리 호일을 집전체로 사용하는 기존의 전극과 비교할 때 약 1.7 배 정도 되는 수치이다. 또한, 탄소부직포를 집전체로 활용하여 전극을 구성했을 때, 충방전 과정 중 전극의 두께 변화나 수명 특성 측면에서 기존의 전극에 비교하여 개선된 성능을 보여주었다.

탄소 부직포의 집전체로 활용가능성을 확장시키기 위해 간편한 활물질 인가 방법을 고안하였다. 점도를 충분히 낮춘 슬러리를 이용하여 침투 공정을 시행하였는데, 이때 직접 제작한 suction 장비 덕분에 위 공정을 성공적으로 진행할 수 있었다. 30 %

의 고형분 비율을 갖는 슬러리를 탄소 부직포 내로 침투시켰고, 이는 약 3분 동안 bar-type method를 통해 가능하였다. 집전체에 비해 약 1.8배 무게의 슬러리를 로딩할 수 있었고, 대부분의 슬러리가 부직포 내부로 침투되었음을 확인하였다. 준비한 전극은 전기화학적으로 뛰어난 성능을 보였으며, 특히 부피당 용량이 크게 개선된 것을 확인하였다.

휨 특성이 뛰어난 음극을 개발하기 위해 $TiO_2$가 코팅된 SUS 부직포를 제작하였다. SUS는 뛰어난 전기전도도를 갖기 때문에 집전체로 활용 가능하다. $TiO_2$는 활물질의 역할을 수행하며, liquid-phase deposition method를 통해 SUS 부직포에 코팅된다. $TiO_2$가 코팅된 SUS 부직포의 휨 특성은 극도의 스트레스를 인가하는 조건인 굽힘 실험을 통해 확인해보았다. 그 결과, 활물질의 탈리가 전혀 발생하지 않으며, 전기화학적인 특성 역시 굽힘 실험 전의 그것과 동일하게 나타나는 것을 확인하였다. 제작한 전극의 훌륭한 휨 특성은 다음의 이유에 기인한다. 가장 먼저, 부직포 형태는 전극을 굽히거나 접으면서 가해지는 스트레스를 효과적으로 분산시킨다고 잘 알려져 있다. 그리고, liquid-phase deposition 도중에 활물질과 집전체는 공유 결합으로 단단히 연결되며, 이는 강력한 계면 결착력을 보장한다. 마지막으로, $TiO_2$라는 활물질은 충방전 도중에 부피 변화를 겪지 않는 물질로 잘 알려져있으며, 이러한 특성은 초기에 확보된 강력한 계면 결착력을 충방전 도중에도 잃지 않게 도와준다. SUS 부직포를 집전체로 활용하여 속도특성이 우수한 전극을 개발했다. Cu foil을 집전체로 활용하여 전극을 구성한 경우와 비교했을 때, 특히 10 C-rate에서 용량 발현 수준에서 큰 차이를 보이는 것을 확인했다. 두 전극의 가장 큰 차이는 집전체의 형태에 있다. SUS 부직포를 집전체로 활용했을 때, 3차원적으로 잘 발달된 전기 전달 경로와 보다 넓은 전극의 표면적을 확보할 수 있으며, 이는 속도특성에 반영된다.

본 연구에서는 활물질의 변화 없이 집전체의 개질만을 통해서 전극의 기존 성능을 강화하거나 새로운 성능을 부여하였다. 집전체 자체에 관한 연구는 많지 않았다.

하지만, 본 연구를 통해 집전체 연구의 이유를 밝힐 수 있었고, 특히 집전체는 전체 전극의 형태를 지배한다는 점에서 앞으로 더욱 활발한 연구가 기대된다.

주 요 어: 리튬 이온 전지, 집전체, 탄소 부직포, 서스 부직포, $Cu_6Sn_5$ 합금, $TiO_2$, liquid-phase deposition, 고용량 음극, 휨 특성이 있는 음극

학 번: 2011-22933